International Journal of Hydrogen Energy 67 (2024) 728–749

Contents lists available at ScienceDirect

International Journal of Hydrogen Energy

journal homepage: www.elsevier.com/locate/he

Multi-time scale scheduling optimization of integrated energy systems considering seasonal hydrogen utilization and multiple demand responses

Zhewei Wang [a], Banghua Du [b], Yang Li [c], Changjun Xie [a,b,*], Han Wang [a], Yunhui Huang [a], Peipei Meng [a]

[a] School of Automation, Wuhan University of Technology, Wuhan, 430070, China
[b] School of automotive engineering, Wuhan University of Technology, Wuhan, 430070, China
[c] Department of Electrical Engineering, Chalmers University of Technology, Gothenburg, 41258, Sweden

ARTICLE INFO

Keywords:
Integrated energy system (IES)
Multi-time scale scheduling
Seasonal hydrogen utilization
Demand response
Ladder-type carbon trading mechanism

ABSTRACT

Hydrogen energy is recognized as a crucial solution for addressing energy crises and advancing energy conservation and emissions reduction. It will play a significant role in the future integrated energy systems (IESs). However, the influence of seasonal variations in scheduling optimization of hydrogen-integrated energy system has rarely been investigated. A low-carbon scheduling model for IES, adopting multiple demand responses and a ladder-type carbon trading mechanism, has been established. Additionally, a multi-time scale dispatch optimization strategy considering seasonal hydrogen utilization is thus proposed in this paper. Specifically, day-ahead scheduling optimizes the system taking into account the seasonal variations of renewable energy and load. In the intraday stage, rolling optimization is adopted to address the forecasting errors introduced by wind and photovoltaic fluctuations. In the real-time stage, chance-constrained methods are employed to ensure short-term supply-demand balance. The efficacy of the proposed strategy is verified using real-world measurements, and the results show the multi-time scale scheduling strategy and multiple demand responses effectively enhanced the system's self-regulation capability, leading to a 12% increase in renewable energy absorption. In addition, seasonal hydrogen utilization is essential for system design, as it enhances the absorption of renewable energy, reducing the purchase cost by 4% and the total cost by 2.6%.

1. Introduction

Energy systems are experiencing a rapid global transition towards a more sustainable and diversified paradigm [1–3]. The large-scale adoption of renewable energy, such as solar and wind, has effectively reduced greenhouse gas emissions and alleviated the pressure from increased energy consumption [4,5]. However, the unsteady and intermittent nature of renewable resources and the limited energy transfer capability cause a significant amount of curtailment of renewable generation every year [6–8]. An integrated energy system (IES) is a promising solution that can provide a platform for these diversified energy conversion processes with high-penetration renewables. Such a system can meet various end-user needs by providing different forms of energy supply, thus achieving highly efficient tiered energy utilization [9–11].

Recently, substantial progress has been made in the design and operation of IESs. Geidl et al. were among the first to propose the system structure of energy hubs [12], based on which substantial research works have been focused on the modeling, planning, and scheduling of IES. For example, in Ref. [13], a graph theory-based standardized matrix modeling method was introduced, which can reduce the nonlinearity in optimization models and facilitate the obtaining of the solution for such a complex system. In Refs. [14–17], different IES structures were proposed and investigated by incorporating multiple forms of energy, such as electricity, gas, heat, and cooling. In Ref. [18], an electricity system integrated large-scale wind power and power to gas (P2G), which focused on the optimal short-term operation to enhance the coupling between natural gas and electrical energy. A novel combined heat and power (CHP) model incorporating P2G and carbon capture and storage (CCS) was proposed in Ref. [19], where both the system's carbon emissions and operational costs were reduced. Reference [20] studied the competitive relationships between multiple market entities in an IES, solving scheduling problems in highly complex energy coupling systems with large-scale renewable energy generation.

Amongst various forms of energy in a modern IES, hydrogen plays a

* Corresponding author. School of Automation, Wuhan University of Technology, Wuhan, 430070, China.
E-mail address: jackxie@whut.edu.cn (C. Xie).

https://doi.org/10.1016/j.ijhydene.2024.04.125
Received 27 January 2024; Received in revised form 21 March 2024; Accepted 10 April 2024
Available online 24 April 2024

significant role in enhancing energy security and promoting the circular economy with a high penetration of renewable generation. By 2050, the demand for hydrogen energy is expected to be tenfold its current level, with its share in China's terminal energy system to reach at least 10%. Due to its widespread availability, environmental friendliness, and zero carbon emissions, effective and efficient generation and utilization of hydrogen energy are indispensable for addressing the long-term issue of climate change and achieving carbon neutrality goals [21–23].

The IESs with hydrogen energy have also been extensively studied. For example, reference [24] established a wind-photovoltaic-hydrogen power integrated model, providing an effective pathway for accommodating renewable energy in IES and ensuring reliable hydrogen supply. In Ref. [25], a methane reactor (MR) was coupled with CCS, and the refined utilization of hydrogen energy was considered on the basis of the traditional P2G, improving the energy efficiency of IES with significant economic, environmental, and technical benefits. In Ref. [26], a hydrogen subsystem consisting of hydrogen tanks and fuel cells was created by separating electrolyzers from P2G, and a dual-layer optimization model was proposed for this IES. This model considered the dynamic market environment involving electricity, hydrogen, and emission exchanges, strengthening system resilience against external disruptions and enhancing the capacity to absorb the generated renewable energy. In Ref. [27], an industry-cluster-based energy management system was constructed to minimize operational costs or maximize the production of green hydrogen. In Ref. [28] , a near-zero carbon IES featuring electricity, heat and hydrogen was constructed, which utilizes a multi-time scale operational optimization to fully capitalize on the advantages of hydrogen hybrid energy storage. It can be seen that the above works focus on constructing suitable IES and optimizing their scheduling strategies based on varying demands, assuming fixed patterns in renewables and loads. However, these studies ignore variations in seasonal climate and load, which will limit the utilization of advantages of hydrogen storage, including long-term storage and cross-regional and cross-seasonal scheduling.

It is worth noting that as the coupling level between various types of energy increases, the devices' output characteristics show more pronounced differences across time scale. The tight coupling and the multiple-source conversion between different energy forms pose considerable challenges to IES scheduling and management. In Ref. [29], electrical and thermal energy storage were utilized as short-term solutions. In contrast, hydrogen storage was employed for long-term use in an integrated energy microgrid, optimizing system scheduling through lifecycle analysis of energy chains. Reference [30] capitalized on the benefits of hybrid energy storage systems in stabilizing power fluctuations and extending storage life, effectively addressing the scheduling issues of combined cooling, heat, and power (CCHP) and other storage devices across different time scales. In Ref. [31], the charging and discharging characteristics of electric vehicles were considered under several typical scenarios with uncertainties, and the IES performance was optimized while ensuring stable grid operation. In Refs. [32,33], adaptive scheduling strategies were explored to match the response delay times of different devices. Their algorithms can enhance the reliability during the operation of multiple-energy systems and effectively handle the uncertainties introduced by wind power generation. In Ref. [34], a multi-time scale game optimization scheduling model for the park-level IES was proposed , which optimized the unit output plan at each time scale through the game behavior of the system and users to motivate users to participate in demand response. The improvement of system operation can be further supported by applying demand response (DR) after analyzing the characteristics of renewable generation/load at different times. For example, DR was implemented in distributed IESs and a multi-temporal and spatial optimization model was established in Ref. [35]. This approach adjusts the load curve through time-shifting and peak-shaving responses, alleviating requirements on the energy supply. In Ref. [36], the changes in user satisfaction caused by load adjustments were considered when industrial users participated in multi-energy DR. The energy costs of industrial production and the dissatisfaction of industrial users were reduced, while the operational efficiency of production equipment and the stability of IES increased. Reference [37] designed a rural IES incorporating transferable DR in the optimization of system operations, and enhanced the match rate between supply and demand as well as the consumption rate of clean energy. Multi-time scale scheduling optimization and DR can adeptly accommodate the diverse characteristics of various types of devices. However, many studies have not analyzed the differences in cross-seasonal scheduling optimization and the synergistic application among different DR strategies, which has been fully considered in this work.

In addition to seasonal hydrogen utilization and DRs, it is well-accepted that carbon trading can provide further enhancement for high energy efficiency, reduce carbon emissions, and improve operational economics, especially in an IES. This technique was investigated in works such as [38,39], where the system costs due to carbon emissions were considered as the optimization objective function. However, these studies designed carbon trading under a fixed price. Such a market mechanism cannot provide sufficient incentives to limit high carbon emissions, whereas adaptive carbon emission regulation is deemed to be more rewarding. Therefore, in Ref. [40], a ladder-type carbon trading mechanism (LTCTM) was proposed for an integrated electricity-gas-heat energy system to strengthen the suppression of carbon emissions, thereby enhancing the low-carbon benefits of IES. In Ref. [41], small modular nuclear power units were introduced into an IES with the LTCTM, where a new low-carbon scheduling model was established to demonstrate good economic and environmental benefits.

In view of the above, few studies have considered the source-load scheduling differences in the seasonal scheduling of IES with hydrogen utilization. As a result, the full potential of hydrogen storage's long duration and large-scale storage capabilities has not been effectively utilized. Furthermore, while some limited studies have considered the time response differences between various devices and DR, these efforts have not optimized the operational characteristics with multiple demand responses at different time scales. Clean units such as P2G and CCS can indeed reduce the carbon emissions of the IES. However, their impact on the total CO_2 emissions needs to be combined with a carbon trading mechanism to address overall system constraints. Hence, this paper proposes a multi-time scale low-carbon scheduling model for the hydrogen-integrated energy system (HIES), incorporating seasonal hydrogen utilization and various load demand response and employing a ladder-type carbon trading mechanism to reduce the carbon emissions. The following merits contribute to the research area, demonstrated using real-world measurement data from a hydrogen energy park in South China.

(1) In the proposed HIES with seasonal utilization, the multiple energy conversion processes through hydrogen fuel cells, methane reactors, and hydrogen-blended gas boilers offer enhanced system scheduling flexibility to consume more renewable energy. It also considers cross-seasonal source-load fluctuations and storage handling to optimize system scheduling results.
(2) The proposed model for scheduling the HIES is designed with three stages at different time scales, i.e., day-ahead, intraday, and real-time, where a piecewise linearization method is utilized for model simplification. Specifically, intraday scheduling is achieved by rolling optimization based on day-ahead planning. At the real-time stage, chance-constrained methods are adopted to ensure the short-time balance between supply and demand.
(3) More types of DR resources are fully utilized to participate in the coordinated operation of the system, achieving coordinated operation on both the supply and demand sides of IES. The response characteristics of different DR types across time scales and energy types are analyzed, providing strategic suggestions from the demand side for the economic operation of IES.

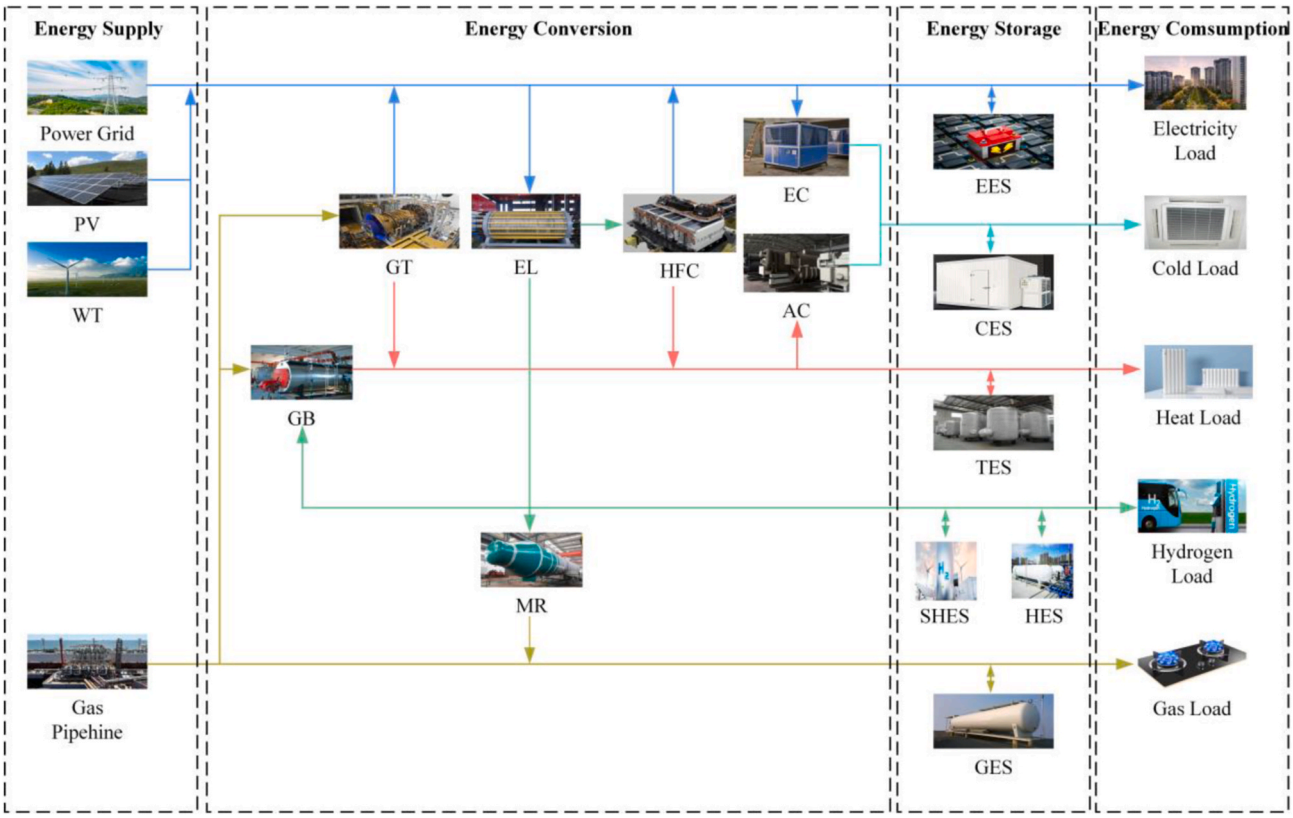

Fig. 1. Structure diagram of HIES.

2. Modeling and operation of a HIES

2.1. System configuration of a HIES

The structure of the HIES under investigation is illustrated in Fig. 1. The system adopts a bus configuration, and five forms of energy are included: electricity, gas, heat, hydrogen, and cooling. This structure can support independent modeling and connection of different power and gas sources, energy storage, and energy conversion devices. It also facilitates the optimization and simulation implementation of the HIES, enhancing the system scheduling's universality and flexibility. The established HIES is divided into four parts: energy supply, energy conversion, energy storage, and energy consumption. The HIES receives electricity and gas from the external power grid and pipeline networks, respectively, to ensure energy supply. It also facilitates the consumption of renewable energy sources (RES) by connecting wind turbines (WT) and photovoltaic (PV) devices to the buses.

The energy conversion mainly consists of a two-stage process: P2G, hydrogen-to-electricity-and-heat, and other energy conversion processes. In the first stage, surplus electrical energy is converted into hydrogen energy using electrolyzers (ELs). In the second stage, the hydrogen energy is further transformed into natural gas chemical energy through MR. The hydrogen-to-electricity-and-heat process involves hydrogen fuel cells (HFC) using electrochemical reactions to convert hydrogen energy into electricity. It supplies heat externally through water cooling. In addition, a hydrogen-blendeded gas boiler (GB) converts chemical energy into heat by burning hydrogen-enriched natural gas. Other energy conversion processes include a gas turbine (GT) transforming natural gas chemical energy into electrical and thermal energy output. Furthermore, an electric chiller (EC) and an absorption chiller (AC) convert electrical and thermal energy, respectively, into cold energy to meet the cold load requirements of the system. Through these processes, inherent physical barriers between different forms of energy are mitigated.

The energy storage comprises electrical energy storage (EES), thermal energy storage (TES), gas energy storage (GES), hydrogen energy storage (HES), and cold energy storage (CES). The energy storage can be used to absorb surplus energy generation effectively, facilitate cross-period energy transfer, balance loads, and smooth out peaks and valleys in the energy profiles. It is worth noting that in the proposed configuration, hydrogen storage devices are categorized into short-term hydrogen energy storage (HES) and seasonal hydrogen energy storage (SHES) based on the usage requirements of hydrogen energy. HES corresponds to meeting short-term direct hydrogen energy demands, where hydrogen gas can be directly supplied to devices such as HFC and MR through gas valves connected outside the hydrogen storage tank. In contrast, the SHES employs low-pressure hydrogen storage tanks, suitable for applications without limitations on size and capable of meeting long-term cross-seasonal energy storage demand.

Finally, energy consumers are the end-users of the system, and the HIES can meet the demands of users for five different forms of energy.

2.2. Modeling of energy equipment

In this section, the mathematical models of all components in the HIES are established and analyzed, including different types of equipment for energy supply, energy conversion, and energy storage, by considering their operational mechanisms and characteristics.

2.2.1. Energy supply

The energy supply equipment includes WT and PV. A WT converts the kinetic energy of wind into mechanical energy in the turbine-generator mass, then transforms it into electrical energy. Therefore, the output power of WT is closely related to wind speed. Due to the uncertainty of wind, WT power is also intermittent and stochastic. The relationship between the output power of the wind turbine P_{wt}^{t} and wind

speed v is described by

$$P_{wt}^{t}=\begin{cases}0 & v^{t}<v_{i} \text{ or } v^{t}<v_{0}\\ \dfrac{(v^{t})^{3}-(v_{i})^{3}}{(v_{r})^{3}-(v_{i})^{3}}\overline{P}_{wt} & v_{i}<v^{t}<v_{\mathrm{r}}\\ \overline{P}_{wt} & v_{r}<v^{t}<v_{0}\end{cases} \tag{1}$$

where $\overline{P}_{wt}$ represents the rated power of WT, and v_r, v_i, and v_0 represent the rated wind speed, cut-in wind speed, and cut-out wind speed of WT, respectively.

The primary factor influencing the PV output power P_{pv} is solar irradiance I. The corresponding relationship can be directly described using a linear equation:

$$P_{pv}^{t}=\eta_{s}SI^{t} \tag{2}$$

where η_s and S represent PV's conversion efficiency and total area, respectively.

2.2.2. Energy conversion

This section includes the modeling of various energy conversion devices such as GT, HFC, EC, AC, EL, GB, and MR. These devices can convert energy generated from the energy supply into a different form that meets various loads, achieving efficient energy utilization. In particular, GT and HFC incorporate waste heat recovery processes, enabling the simultaneous supply of electrical and thermal energy to the external environment, thereby enhancing the overall efficiency of the system. Due to the fact that the flame temperature of hydrogen is nearly 300 °C higher than that of natural gas and its ignition delay time is over three times shorter than that of natural gas, the hydrogen-blendeded gas boiler is employed. Different from the boilers, which only burn natural gas, the hydrogen-blendeded gas boiler can further reduce carbon dioxide emissions by around 10%, making it more energy-efficient and environmentally friendly. The energy conversion processes of these devices are described by

$$\begin{cases}\begin{cases}P_{gt,e}^{t}=\eta_{gt,e}P_{gt,g}^{t}\varphi_{g}\\ P_{gt,t}^{t}=\eta_{gt,t}\left(1-\eta_{gt,e}\right)P_{gt,g}^{t}\varphi_{g}\end{cases}\\ \begin{cases}P_{hfc,e}^{t}=\eta_{hfc,e}P_{hfc,h}^{t}\varphi_{h}\\ P_{hfc,t}^{t}=\eta_{hfc,t}\left(1-\eta_{hfc,e}\right)P_{hfc,h}^{t}\varphi_{h}\end{cases}\\ P_{ec,c}^{t}=\eta_{ec}P_{ec,e}^{t}\\ P_{ac,c}^{t}=\eta_{ac}P_{ac,t}^{t}\\ P_{el,h}^{t}=\eta_{el}P_{el,e}^{t}\\ P_{gb,t}^{t}=\eta_{gb}\left(P_{gb,h}^{t}+P_{gb,g}^{t}\right)\\ P_{mr,g}^{t}=\eta_{mr}P_{mr,h}^{t}\end{cases} \tag{3}$$

where $P_{gt,e}^{t}$ and $P_{gt,t}^{t}$ represent the output electrical power and thermal power of the GT at time t, respectively; $\eta_{gt,e}$ and $\eta_{gt,t}$ represent the corresponding electrical efficiency and thermal efficiency, respectively; $P_{gt,g}^{t}$ represents the natural gas consumption of the GT; φ_g is the lower heating value of natural gas; $P_{hfc,e}^{t}$ and $P_{hfc,t}^{t}$ represent the output electrical power and thermal power of the HFC, respectively; $\eta_{hfc,e}$ and $\eta_{hfc,t}$ represent the corresponding electrical efficiency and thermal efficiency of the HFC; $P_{hfc,h}^{t}$ is the hydrogen consumption of the HFC; φ_h is the lower heating value of hydrogen; $P_{ec,c}^{t}$, $P_{ec,e}^{t}$, and η_{ec} represent the output cold power, consumed electrical power and cooling efficiency of the EC, respectively; $P_{ac,c}^{t}$, $P_{ac,t}^{t}$, and η_{ac} represent the output cold power, consumed thermal power and cooling efficiency of the AC, respectively; $P_{el,h}^{t}$, $P_{el,e}^{t}$, and η_{el} represent the hydrogen production quantity, input electrical power, and hydrogen production efficiency of the EL, respectively; $P_{gb,t}^{t}$, $P_{gb,h}^{t}$, $P_{gb,g}^{t}$, and η_{gb} represent the thermal power output, hydrogen consumption, natural gas consumption and thermal efficiency of the GB, respectively; $P_{mr,g}^{t}$, $P_{mr,h}^{t}$, and η_{mr} represent the natural gas production quantity, hydrogen consumption, and conversion efficiency of the MR, respectively.

2.2.3. Energy storage

Energy storage is used to smoothen the output of renewable energy, support peak shaving, and improve system stability through planned charging and discharging. The integration of hybrid energy storage technologies allows them to complement each other and effectively increases renewable energy generation in both the short and long terms. It also enhances the overall utilization efficiency, further reducing the operational costs of HIES. The considered energy storage includes EES, TES, GES, HES, and CES. Here, we differentiate the hydrogen storage devices between normal HES and SHES, meeting the daily hydrogen energy scheduling needs and long-term hydrogen energy consumption requirements. The models for energy storage are as follows:

$$E_{m}^{t+1}=\begin{cases}E_{m}^{t}(1-\theta_{m})+P_{m,c}^{t}\eta_{m,c}\Delta t\\ E_{m}^{t}(1-\theta_{m})-P_{m,d}^{t}\Delta t\Big/\eta_{m,d}\end{cases} \tag{4}$$

where $m\in\{ees,ges,tes,hes,shes,ces\}$ represents the type of energy storage; $P_{m,c}^{t}$ and $P_{m,d}^{t}$ are the charging and discharging power of device m at time t, respectively, which cannot occur at the same time; $\eta_{m,c}$ and $\eta_{m,d}$ represent the charging and discharging efficiencies, respectively; θ_m represents the energy loss coefficient; E_m^t and E_m^{t+1} represent current and next-step states of stored energy, respectively; Δt is the time step.

2.3. Carbon trading mechanism

As a crucial component of climate finance, the development of the carbon market is of significant importance for clarifying carbon emission rights and promoting the low-carbon and green development of industries. In order to highlight the contributions of HIES to energy conservation, emissions reduction, and low-carbon operation, this paper adopts the ladder-type carbon trading mechanism. Carbon emissions resulting from higher-level power and those generated by energy conversion equipment are subject to rewards and penalties in the form of carbon trading rights. Furthermore, a quantitative assessment subsidy is provided for the carbon recovery benefits of the MR, which is included in the HIES economic cost model.

The LTCTM billing system prices carbon emissions based on intervals over a certain period of time. As carbon emissions increase, the carbon trading price gradually rises, incentivizing proactive reductions in carbon emissions during system dispatch optimization. The billing baseline for system carbon emissions can be expressed as

$$\overline{EM}_{CO_2}=\sum_{X}\sum_{T}\omega_{x}P_{x}^{t} \tag{5}$$

where P_x^t represents the equivalent electrical load of HIES demand energy $x\in\{e,g,t\}$ at time t; ω_x represents the free carbon emission quota coefficient for energy form x.

The actual carbon emissions of the HIES consist of three parts: the 'virtual carbon emissions' caused by purchased electricity, the emissions from coupled equipment operation, and the carbon recovery from the MR. The actual carbon emissions of the system can be expressed as

Fig. 2. Strategies of multiple demand response.

$$\begin{cases} EM_{CO_2,a} = EM_{grid} + EM_{total} - EM_{mr} \\ EM_{grid} = \sum_{T}\left(a_1 + b_1 P^t_{buy,e} + c_1\left(P^t_{buy,e}\right)^2\right) \\ EM_{total} = \sum_{T}\left(a_2 + b_2 P^t_{totla} + c_2\left(P^t_{totla}\right)^2\right) \\ P^t_{totla} = \sum_{N}\left(P^t_n\right) \\ EM_{mr} = \sum_{T}\varpi P^t_{mr,g} \end{cases} \tag{6}$$

where EM_{grid} represents the virtual carbon emissions from higher-level power purchases; EM_{total} is the actual carbon emissions from energy conversion equipment; EM_{mr} is the actual carbon recovery from the MR; $P^t_{buy,e}$ is the power of electricity purchases at time t; P^t_{totla} is the equivalent output power of energy conversion equipment at time t; P^t_n is the output power of energy conversion equipment $n \in \{gt, gb\}$ at time t; ϖ is the carbon recovery efficiency of the MR. Based (5) and (6), the carbon emissions EM_{CO_2} of the HIES participating in the carbon trading market and the cost of establishing LTCTM can be calculated by the following two equations, namely

$$EM_{CO_2} = EM_{CO_2,a} - \overline{EM}_{CO_2} \tag{7}$$

$$f_{CO_2} = \begin{cases} \lambda EM_{CO_2} & EM_{CO_2} \leqslant l \\ \lambda(1+\alpha)(EM_{CO_2} - l) + \lambda l & l \leqslant EM_{CO_2} \leqslant 2l \\ \lambda(1+2\alpha)(EM_{CO_2} - 2l) + \lambda(2+\alpha)l & 2l \leqslant EM_{CO_2} \leqslant 3l \\ \lambda(1+3\alpha)(EM_{CO_2} - 3l) + \lambda(3+3\alpha)l & 3l \leqslant EM_{CO_2} \leqslant 4l \\ \lambda(1+4\alpha)(EM_{CO_2} - 4l) + \lambda(4+6\alpha)l & EM_{CO_2} \geqslant 4l \end{cases} \tag{8}$$

where f_{CO_2} represents the total cost of carbon trading for the HIES; λ is the carbon trading base price; α is the carbon trading price growth rate; l is the length of the carbon emission interval. In (8), the billing system divides carbon emission quotas into five price intervals. The more quotas are allocated, the higher the price range for carbon trading is. In the model, this is represented by a larger calculation slope for carbon trading costs. Therefore, the higher price ranges are more sensitive to price increases. Compared to traditional fixed carbon emission trading mechanisms, during system dispatch optimization, more consideration will be given to running equipment in low-carbon emission price intervals to achieve the overall goal of low-carbon and energy-efficient operation of the HIES.

2.4. Multi-time scale demand response strategy

DR is divided into spontaneous demand response (SDR) and incentive-based demand response (IDR). SDR is initiated by the load based on practical conditions. Users spontaneously adjust their energy usage time in response to price changes, leading to price-based demand response (PDR). If users change the type of load due to changes in load supply, it is referred to as the alternative demand response (ADR). IDR involves suppliers and users signing relevant agreements in advance, allowing direct control of load power and providing users with corresponding compensation when necessary, which can achieve flexible resource scheduling for demand response. DR from a variety of types of loads usually exhibit a multi-time scale nature. To ensure the full participation of DR and the smooth operation of system scheduling, we design different DR strategies across multiple time scales. Specifically, in the day-ahead stage, the focus is on PDR and ADR, with preliminary optimization of electrical and gas loads. In the intraday stage, ADR and IDR are considered, leading to layered load responses. Finally, in the

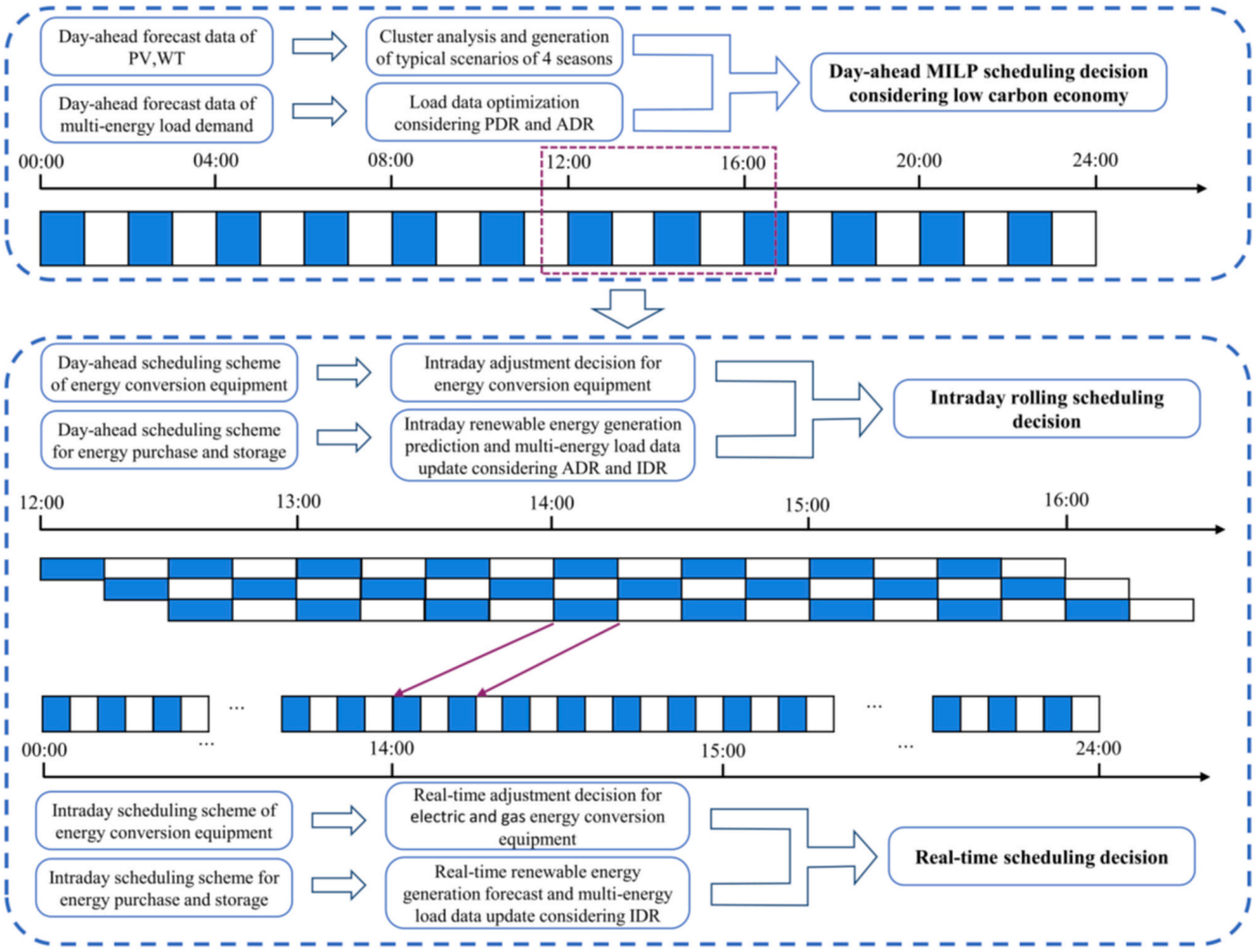

Fig. 3. Multi-time scale scheduling optimization model for HIES.

real-time stage, additional attention is paid to IDR, ensuring precise control over the load. The adopted strategies of multiple demand response are illustrated in Fig. 2.

2.4.1. Price-based demand response

Electricity and gas energy possess commodity attributes. According to microeconomic theory, differences in energy prices can influence changes in user energy consumption. By calculating the ratio of energy prices to corresponding changes, a price elasticity matrix can be established, including both own-price elasticity and cross-price elasticity coefficients [42].

$$M_x = \begin{bmatrix} m_x^{11} & m_x^{12} & \cdots & m_x^{1j} \\ m_x^{21} & m_x^{22} & \cdots & m_x^{2j} \\ \vdots & \vdots & \ddots & \vdots \\ m_x^{i1} & m_x^{i2} & \cdots & m_x^{ij} \end{bmatrix} \tag{9}$$

$$m_x^{ii} = \frac{\Delta L_{PDR,x}^{i}}{\overline{L}_{PDR,x}^{i}} \left(\frac{c_x^i - \overline{c}_x^i}{c_x^i} \right)^{-1} \tag{10}$$

$$m_x^{ij} = \frac{\Delta L_{PDR,x}^{i}}{\overline{L}_{PDR,x}^{i}} \left(\frac{c_x^j - \overline{c}_x^j}{c_x^j} \right)^{-1} \tag{11}$$

where M_x represents the price elasticity matrix for energy and $x \in \{e,g\}$; m_x^{ii} is the own-price elasticity coefficient; m_x^{ij} is the cross-price elasticity coefficient; c_x^i, $\overline{c}_x^i$ and c_x^j, $\overline{c}_x^j$ are the energy prices at times i and j with and without the PDR, respectively; $\overline{L}_{PDR,x}^{i}$ and $\Delta L_{PDR,x}^{i}$ are the load demand without the PDR and the load change at time i.

In multiple periods, the price load response behavior of users can be modeled as follows:

$$L_{PDR,x}^{t} = \left(1 + \overline{L}_{PDR,x}^{t}\right) \sum_{t'} \left(M_x(t,t') \cdot \left(p_x^{t'} - \overline{p}_x^{t'}\right) / \overline{p}_x^{t'}\right) \tag{12}$$

where $L_{PDR,x}^{t}$ represents the load demand at time t with PDR; $p_x^{t'}$ and $\overline{p}_x^{t'}$ represent the energy prices at time t' with and without the PDR, respectively.

2.4.2. Alternative demand response

The HIES consists of five types of energy loads, and users can utilize ADR to change energy consumption patterns based on seasonal variations and different energy supply levels. This achieves lateral complementary substitution for different energy loads. The response model is given by [43].

$$\begin{bmatrix} L_{ADR,e}^{t} \\ L_{ADR,g}^{t} \\ L_{ADR,t}^{t} \\ L_{ADR,h}^{t} \\ L_{ADR,c}^{t} \end{bmatrix} = \begin{bmatrix} 0 & k_{ge} & k_{te} & k_{he} & k_{ce} \\ k_{eg} & 0 & k_{tg} & k_{hg} & k_{cg} \\ k_{et} & k_{gt} & 0 & k_{ht} & k_{ct} \\ k_{eh} & k_{gh} & k_{th} & 0 & k_{ch} \\ k_{ec} & k_{gc} & k_{tc} & k_{hc} & 0 \end{bmatrix} \cdot \begin{bmatrix} \overline{L}_{ADR,e}^{t} \\ \overline{L}_{ADR,g}^{t} \\ \overline{L}_{ADR,t}^{t} \\ \overline{L}_{ADR,h}^{t} \\ \overline{L}_{ADR,c}^{t} \end{bmatrix} + \begin{bmatrix} \overline{L}_{ADR,e}^{t} \\ \overline{L}_{ADR,g}^{t} \\ \overline{L}_{ADR,t}^{t} \\ \overline{L}_{ADR,h}^{t} \\ \overline{L}_{ADR,c}^{t} \end{bmatrix} \tag{13}$$

where $L_{ADR,x}^{t}$ represents the load demand with the ADR at time t; $\overline{L}_{ADR,x}^{t}$

represents the load demand without the ADR at time t; k_{xy} represents the substitutability efficiency between energy x and y, $k_{xy} = -1/k_{yx}$, $x, y \in \{e, g, t, h, c\}$ and $x \neq y$.

2.4.3. Incentive-based demand response

IDR mainly considers interruptible load (IL) and convertible load (CL). IDR has a fast response speed to meet the requirements of rapid load in daily and real-time scenarios. The response model is expressed as

$$L^t_{IDR,x} = \overline{L}^t_{IDR,x} + \Delta L^t_{CL,x} + \Delta L^t_{IL,x} \tag{14}$$

where $L^t_{IDR,x}$ and $\overline{L}^t_{IDR,x}$ represent the load demand of energy form $x \in \{e, g, t, h, c\}$ with and without the IDR at time t, respectively; $\Delta L^t_{CL,x}$ and $\Delta L^t_{IL,x}$ represent the response quantities of CL and IL at time t, respectively.

3. Multi-time scale optimization operation model of the HIES

This section establishes a multi-time scale scheduling optimization model for HIES, as shown in Fig. 3. The day-ahead scheduling solves the output plan for the system's equipment for the next 24 h, with a time interval of 1 h. Intraday scheduling rolls optimization on the basis of the day-ahead results to smooth out the planning errors caused by RES and load uncertainty, with a time interval of 15 min. The real-time scheduling process uses the chance-constrained method to ensure supply and demand balance in a short time, with a time interval of 5 min. At this stage, seasonal energy storage cannot meet the rapid energy scheduling demand and is treated as a constant value. By coordinating these three levels, the HIES can achieve optimized operation across multiple time scales and multiple energy flows.

3.1. Day-ahead scheduling optimization model

3.1.1. Clustering and scenario generation

The wind and solar forecast data for HIES scheduling optimization reference historical weather and operational data from the monsoon climate region in South China. A series of modeling and k-means clustering analyses were conducted, representing the characteristics as typical days for each season. The all-year load data were summarized to extract the wind and solar characteristic curves for four typical days corresponding to spring, summer, autumn, and winter. These curves serve as reference data for the RES input, aiming to characterize the impact of cross-seasonal environmental changes. The reader is referred to Ref. [44] for detailed explanations.

3.1.2. Objective function

In order to improve the economic and environmental performance of the HIES, we formulate the daily operational costs of HIES as an objective function for scheduling optimization. This cost consists of energy purchase cost f^d_{buy}, equipment maintenance cost f^d_{om}, carbon emission cost $f^d_{CO_2}$, curtailed wind and solar cost f^d_{ab}, and load loss penalty cost f^d_{loss}. The optimization problem can be expressed as follows:

$$\min f^d = f^d_{buy} + f^d_{om} + f^d_{CO_2} + f^d_{ab} + f^d_{loss} \tag{15}$$

$$\begin{cases} f^d_{buy} = \sum_T \left(c_e P^t_{buy,e} + c_g P^t_{buy,g} \right) \\ f^d_{om} = \sum_T \sum_N \left(k_{om,n} P^t_n \right) \\ f^d_{ab} = \sum_T \left(k_{ab,PV} P^t_{ab,PV} + k_{ab,WT} P^t_{ab,WT} \right) \\ f^d_{loss} = \sum_T \sum_X \left(k_{loss,x} L^t_{loss,x} \right) \end{cases} \tag{16}$$

where f^d_{buy} represents the system's pre-scheduling stage energy purchase cost; $P^t_{buy,g}$ is the gas purchase quantity for the HIES at time t; P^t_n is the output power of energy conversion equipment $n \in \{gt, hfc, ec, ac, el, gb, mr\}$; $k_{om,n}$ is the corresponding equipment cost coefficient; $P^t_{ab,PV}$ and $P^t_{ab,WT}$ are the curtailed wind and solar power for the system, respectively; $k_{ab,PV}$ and $k_{ab,WT}$ are the respective penalty coefficients for curtailed wind and solar, respectively; $L^t_{loss,x}$ is the system's load loss; and $k_{loss,x}$ is the penalty coefficient for load loss.

3.1.3. Constraints

The constraints in the day-ahead scheduling stage mainly include energy balance constraints, energy purchase constraints, and equipment operation constraints in both time and space.

3.1.3.1. Energy balance constraints.

$$\begin{cases} P^t_{buy,e} + P^t_{PV} - P^t_{ab,PV} + P^t_{WT} - P^t_{ab,WT} + P^t_{gt,e} + P^t_{hfc,e} - P^t_{ess,c} + P^t_{ess,d} = L^t_{DR,e} - L^t_{loss,e} + P^t_{el,e} + P^t_{ec,e} \\ P^t_{buy,g} + P^t_{mr,g} - P^t_{ges,c} + P^t_{ges,d} = L^t_{DR,g} - L^t_{loss,g} + P^t_{gt,g} + P^t_{gb,g} \\ P^t_{gb,t} + P^t_{gt,t} + P^t_{hfc,t} - P^t_{tes,c} + P^t_{tes,d} = L^t_{DR,t} - L^t_{loss,t} + P^t_{ac,t} \\ P^t_{el,h} - P^t_{shes,c} + P^t_{shes,d} - P^t_{hes,c} + P^t_{hes,d} = L^t_{DR,h} - L^t_{loss,h} + P^t_{hfc,h} + P^t_{gb,h} + P^t_{mr,h} \\ P^t_{ec,c} + P^t_{ac,c} - P^t_{tes,c} + P^t_{tes,d} = L^t_{DR,c} - L^t_{loss,c} \end{cases} \tag{17}$$

where $L^t_{DR,x}$ represents the load demand of energy $x \in \{e, g, t, h, c\}$ at time t with DR.

3.1.3.2. Energy purchase constraints

$$\begin{cases} 0 \leqslant P^t_{buy,e} \leqslant P_{buy,e,\max} \\ 0 \leqslant P^t_{buy,g} \leqslant P_{buy,g,\max} \end{cases} \tag{18}$$

where $P_{buy,e,\max}$ and $P_{buy,g,\max}$ represent the maximum purchased electricity and gas quantities for the system, respectively.

3.1.3.3. Equipment operation constraints. In the HIES, the equipment includes energy conversion devices and energy storage devices. The operational constraints for energy conversion devices include upper and lower limits on device operating power and ramping, i.e.,

$$0 \leqslant P^t_n \leqslant P_{n,\max} \tag{19}$$

$$0 \leqslant P^{t+1}_n - P^t_n \leqslant \delta P_{n,\max} \tag{20}$$

where $P_{n,\max}$ and $\delta P_{n,\max}$ are the upper limits of the power and ramping constraint of the energy conversion device $n \in \{gt, hfc, ec, ac, el, gb, mr\}$, respectively.

Due to the use of hydrogen-blendeded gas as fuel in GB, the heat

released from hydrogen combustion is higher compared to an equal amount of natural gas. To ensure the safe operation of the equipment and avoid significant structural modifications to the equipment itself, strict limitations are imposed on the proportion of hydrogen. The maximum proportion of hydrogen power to the total is considered as 0.3:

$$0 \leqslant P^t_{gb,h} \Big/ \left(P^t_{gb,h} + P^t_{gb,g}\right) \leqslant 0.3 \tag{21}$$

In addition to the upper and lower limits on charging and discharging, the constraints on energy storage devices also include capacity constraints.

$$\begin{cases} E_{m,\min} \leqslant E^t_m \leqslant E_{m,\max} \\ 0 \leqslant P^t_{m,c} \leqslant \lambda_{m,c} P_{m,c,\max} \\ 0 \leqslant P^t_{m,d} \leqslant \lambda_{m,d} P_{m,d,\max} \\ \lambda_{m,c} + \lambda_{m,d} = 1 \end{cases}, i = 1,2,3 \tag{22}$$

where $E_{m,\max}$ and $E_{m,\min}$ represent the capacity upper and lower limits of energy storage device $m \in \{ees, ges, tes, hes, shes, ces\}$, respectively. $P_{m,c,\max}$ and $P_{m,d,\max}$ represent the maximum charging and discharging power of energy storage device m, respectively; $\lambda_{m,c}$ and $\lambda_{m,d}$ are binary variables representing the charging and discharging states of energy storage devices, respectively.

Considering the continuity of the energy storage dispatch period, the states of other types of energy storage, excluding the SHES, should remain consistent at the beginning and end of the dispatch cycle. Furthermore, the initial and final states of SHES must also be consistent throughout the annual dispatch cycle. These give

$$E^0_m = E^{24}_m \tag{23}$$

$$E^0_{shes} = E^T_{shes} \tag{24}$$

3.2. Intraday rolling scheduling optimization model

3.2.1. Stochastic uncertainty of RES and load

In the intraday scheduling phase, due to the decreasing uncertainty of renewable energy and load power with the shortening of the time scale, a normal distribution is employed to model the intraday prediction errors of the RES and load, as shown below.

$$\begin{cases} f\left(\xi^i_{wt}\right) = \dfrac{1}{\sigma_{wt}\sqrt{2\pi}} e^{-\left(\xi^i_{wt} - \mu_{wt}\right)^2 \Big/ 2\sigma^2_{wt}} \\ f\left(\xi^i_{pv}\right) = \dfrac{1}{\sigma_{pv}\sqrt{2\pi}} e^{-\xi^{i2}_{pv} \Big/ 2\sigma^2_{pv}} \\ f\left(\xi^i_L\right) = \dfrac{1}{\sigma_L\sqrt{2\pi}} e^{-\xi^{i2}_L \Big/ 2\sigma^2_L} \end{cases} \tag{25}$$

where ξ^i_{wt}, ξ^i_{pv} and ξ^i_L are the intraday power deviations for WT, PV, and load, respectively; μ_{wt}, σ_{wt}, σ_{pv}, and σ_L are the corresponding distribution coefficients.

3.2.2. Objective function

In the intraday scheduling stage, based on the results of the day-ahead scheduling, the adjustment costs f^i_{ad} of HIES in each scheduling period and the additional operational costs f^i_{IDR} due to IDR adjustments are considered in the objective function (26):

$$\min f^i = f^i_{buy} + f^i_{om} + f^i_{CO_2} + f^i_{ab} + f^i_{loss} + f^i_{ad} + f^i_{IDR} \tag{26}$$

$$\begin{cases} f^i_{ad} = \sum_T \sum_N \left(k_{ad,n} \Delta P^t_n\right) \\ f^i_{IDR} = \sum_T \left(c_{IL,x} \left|\Delta L^t_{IL,x}\right| + c_{CL,x} \left|\Delta L^t_{CL,x}\right|\right) \end{cases} \tag{27}$$

where $k_{ad,n}$ is the adjustment cost coefficient for energy conversion devices; ΔP^t_n is the power adjustment of energy conversion devices at time t; f^i_{IDR} is the subsidy cost of IDR in the intraday scheduling stage; $c_{IL,x}$ and $c_{CL,x}$ are the unit subsidy prices for IL and CL for energy x.

3.2.3. Constraints

The intraday rolling optimization model involves all devices responding within 15 min, and the constraints include energy balance constraints (17), energy purchase constraints (18), and equipment operation constraints (19)-(24)-(24). In addition, IDR constraints and power adjustment constraints for energy conversion devices need to be considered.

$$\begin{cases} 0 \leq \Delta L^t_{IL,x} \leq \Delta L^t_{IL,x,\max} \\ 0 \leq \Delta L^t_{CL,x} \leq \Delta L^t_{CL,x,\max} \end{cases} \tag{28}$$

$$0 \leq \Delta P^t_n \leq \Delta P^t_{n,\max} \tag{29}$$

where $\Delta L^t_{IL,x,\max}$ and $\Delta L^t_{CL,x,\max}$ represent the maximum response quantities of IL and CL corresponding to energy x, respectively; $\Delta P^t_{n,\max}$ is the upper limit of the adjustment quantity for coupled device n.

3.3. Real-time stochastic scheduling optimization model

3.3.1. Chance-constrained scheduling optimization

In the real-time scheduling stage, short-term prediction errors of the RES and load power are modeled using a normal distribution. The fluctuation amplitude is small at this stage. Therefore, this paper adopts the chance-constrained programming(CCP) to ensure that the probability of constraint conditions holding is not less than a certain confidence level when optimizing system scheduling based on the objective function.

3.3.2. Objective function

The short-response devices with faster response in the HIES take priority in participating in real-time scheduling optimization adjustments, while the SHES does not participate in this stage of scheduling. The objective function is:

$$\min f^r = f^r_{buy} + f^r_{om} + f^r_{CO_2} + f^r_{ab} + f^r_{loss} + f^r_{ad} + f^r_{IDR} + f^r_{es} \tag{30}$$

$$f^r_{es} = \sum_T \sum_M \left(k_{es,m} \Delta P^t_m\right) \tag{31}$$

where f^r_{es} represents the real-time stage energy storage adjustment cost, ΔP^t_m is the power adjustment of energy storage device m, and $k_{es,m}$ is the adjustment cost coefficient of energy storage device m.

3.3.3. Constraints

In the real-time optimization model, the chance-constrained method is employed. The control of energy storage devices only needs to meet the supply rates of various loads at their respective confidence levels. The remaining slight deviations can be compensated by real-time purchasing from upper-level electricity, gas, and load adjustment. Therefore, the constraint conditions at this stage are similar to the energy purchase constraints (18), equipment operation constraints (19)-(24) and DR constraints (28)-(29), while the difference is that the following chance constraints are applied instead of the deterministic constraints, i.e.,

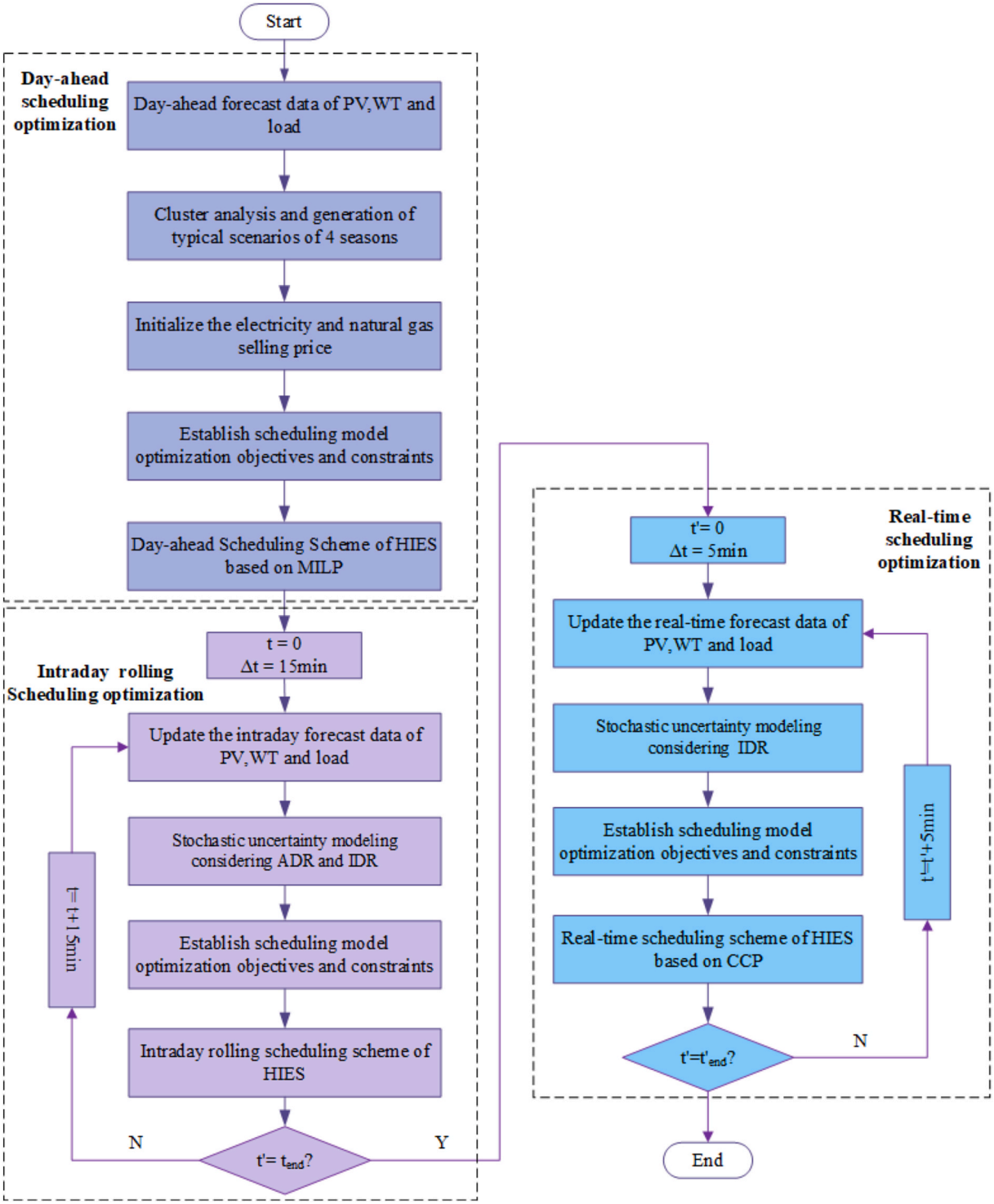

Fig. 4. Multi-time scale scheduling optimization flowchart.

Table 1
Scenarios for day-ahead optimization scheduling for HIES.

Scenario	P2G	P2H	SHES	Fixed CTM	LTCTM
1			✓		✓
2	✓	✓			✓
3	✓		✓		✓
4	✓	✓	✓		
5	✓	✓	✓	✓	
6	✓	✓	✓		✓

$$\begin{cases} \Pr\left\{ \begin{array}{l} P^t_{buy,e}+P^t_{PV}-P^t_{ab,PV}+P^t_{WT}-P^t_{ab,WT}+P^t_{gt,e}+P^t_{hfc,e}-P^t_{ess,c}+P^t_{ess,d} \\ =L^t_{DR,e}-L^t_{loss,e}+P^t_{el,e}+P^t_{ec,e} \end{array} \right\} \geq \beta_1 \\ \Pr\left\{ P^t_{buy,g}+P^t_{mr,g}-P^t_{ges,c}+P^t_{ges,d}=L^t_{DR,g}-L^t_{loss,g}+P^t_{gt,g}+P^t_{gb,g} \right\} \geq \beta_2 \\ \Pr\left\{ P^t_{gb,t}+P^t_{gt,t}+P^t_{hfc,t}-P^t_{tes,c}+P^t_{tes,d}=L^t_{DR,t}-L^t_{loss,t}+P^t_{ac,t} \right\} \geq \beta_3 \\ \Pr\left\{ P^t_{el,h}-P^t_{shes,c}+P^t_{shes,d}-P^t_{hes,c}+P^t_{hes,d}=L^t_{DR,h}-L^t_{loss,h}+P^t_{hfc,h}+P^t_{gb,h}+P^t_{mr,h} \right\} \geq \beta_4 \\ \Pr\left\{ P^t_{ec,c}+P^t_{ac,c}-P^t_{tes,c}+P^t_{tes,d}=L^t_{DR,c}-L^t_{loss,c} \right\} \geq \beta_5 \end{cases} \tag{32}$$

Where the probability Pr{} represents the confidence level, and $\beta_i = 0.95$ is the designed confidence level of power balance.

4. Case study

4.1. Solution method

Fig. 4 shows the process of optimizing scheduling strategies at multiple time scales proposed in this article. Clearly, the LTCTM model, which includes segmented functions and quadratic terms, makes the HIES a typical mixed integer nonlinear programming (MINLP) model. Metaheuristic optimization can be readily applied to solve this MINLP model, but it usually requires a heavy computational load and significant computational resources. To facilitate rapid computation and online applications, we propose first to carry out piecewise linearization and transform the model into a mixed integer linear programming (MILP) model, then call the software package Yalmip in the CPLEX

Table 2
Day-ahead optimization scheduling results of HIES in different cases.

Scenario	Purchase cost (¥)	Maintenance cost (¥)	Curtailed wind and light (%)	Load loss (kW)	Carbon emissions (kg)	Total cost (¥)
1	13,804	1076	0.89	917	11,636	28,114
2	15,301	1426	0.25	0	10,412	20,091
3	14,012	1244	0.16	917	9758	27,519
4	14,225	1308	0.30	0	12,179	24,707
5	14,331	1342	0.27	0	11,637	19,782
6	14,679	1416	0.20	0	10,659	19,576

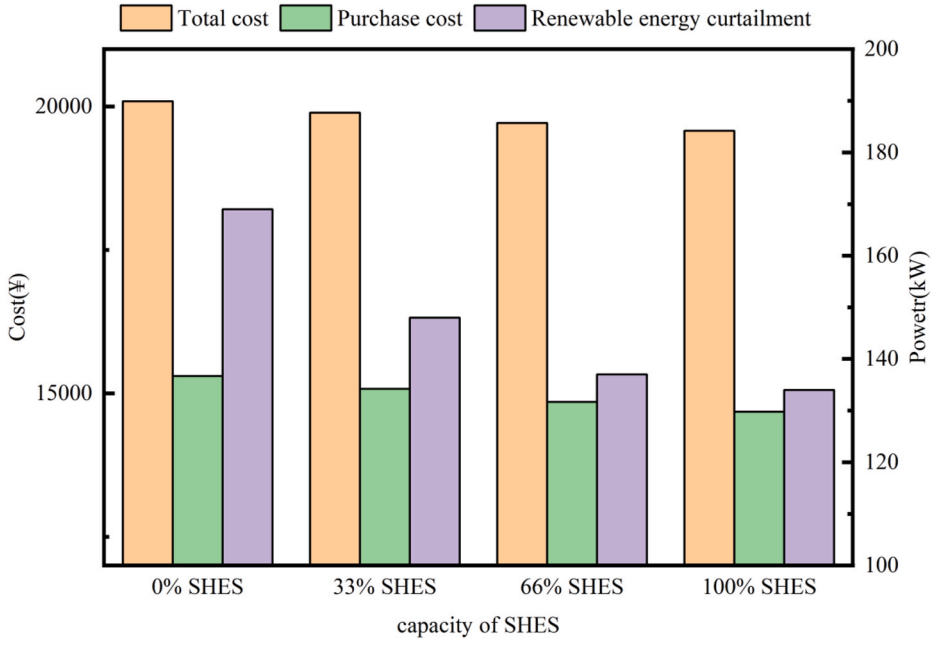

Fig. 5. Optimization results of the system with different seasonal hydrogen storage capacity.

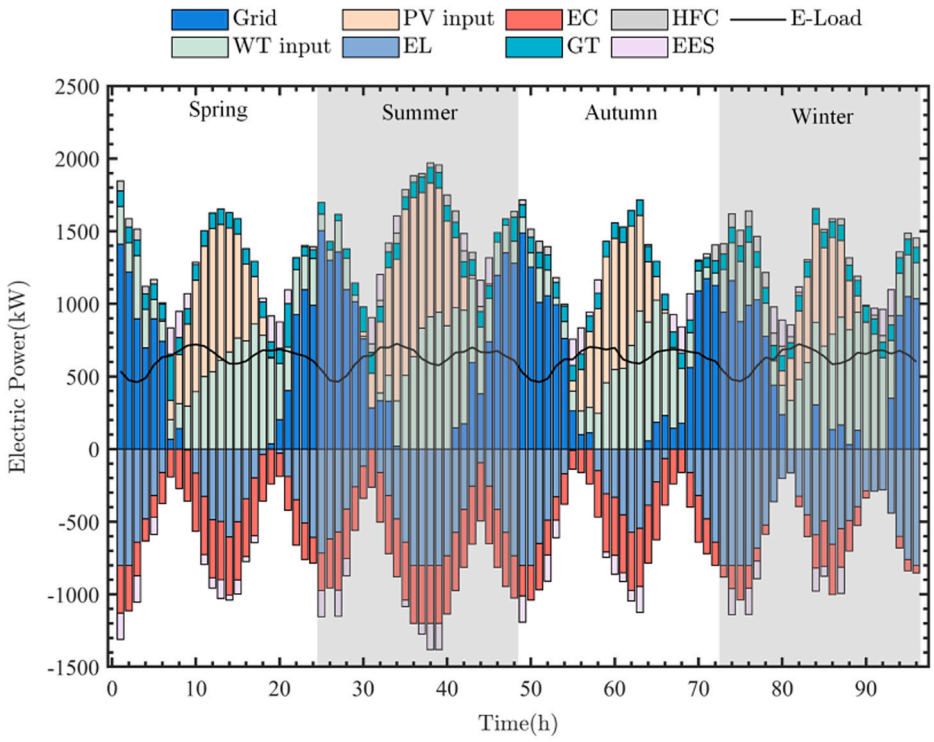

(a) Electric power balance

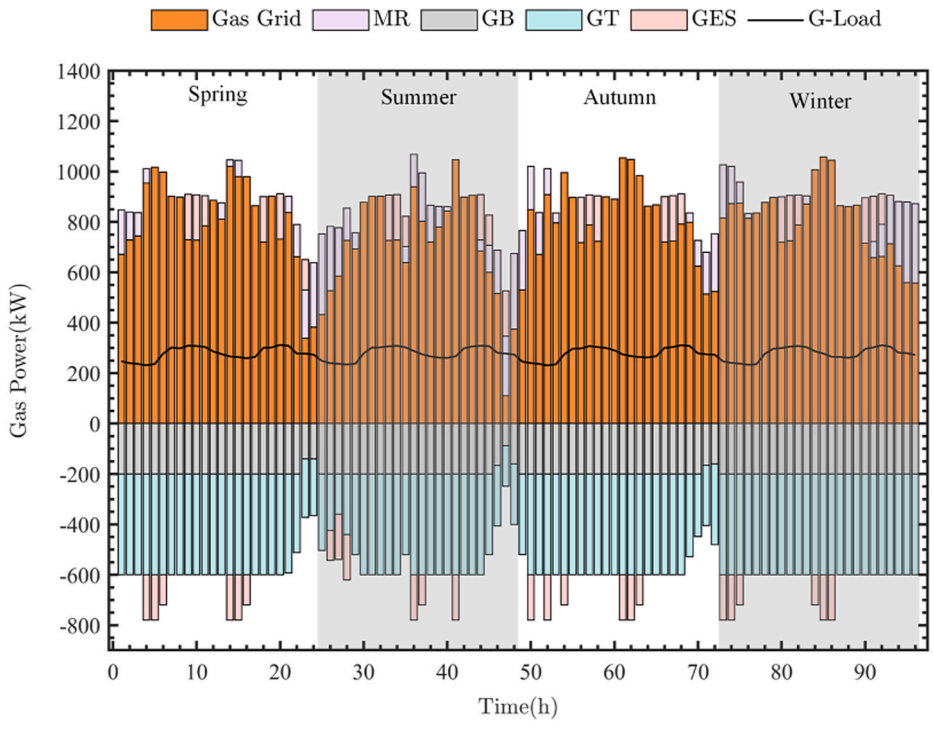

(b) Gas power balance

Fig. 6. Energy supply and demand scheduling results of HIES in the day-ahead stage.

commercial solver. Specific model parameters and the linearization process are detailed in Appendix A.

4.2. Day-ahead scheduling analysis

To analyze the impact of seasonal hydrogen energy utilization and the LTCTM on HIES operations, six scenarios were established for comparative analysis in the day-ahead stage. These scenarios are.

Scenario 1: Comprehensive utilization of hydrogen energy is not considered. Hydrogen generated by the EL is only used to meet the hydrogen load demand of the system.

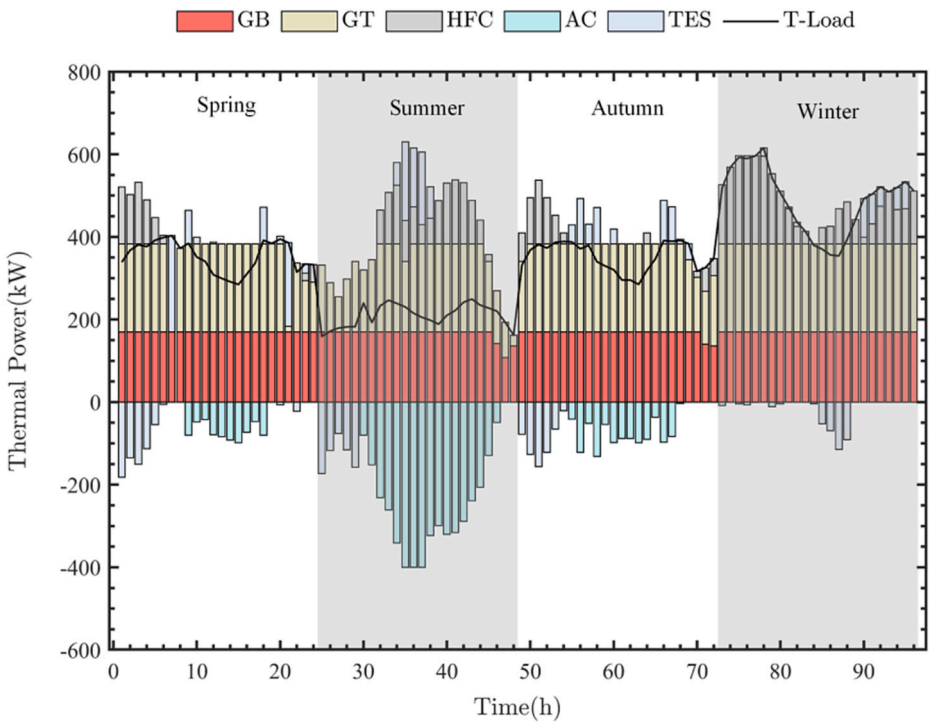

(c) Thermal power balance

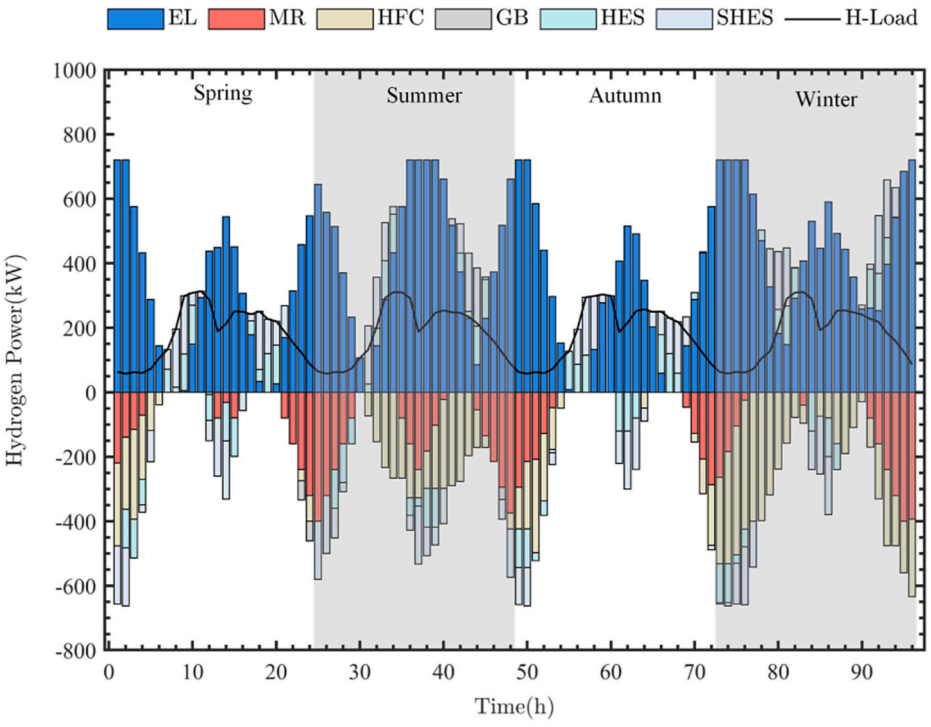

(d) Hydrogen power balance

Fig. 6. (*continued*).

Scenario 2: Seasonal hydrogen storage is not considered when employing the LTCTM scheme.
Scenario 3: The Power-to-Hydrogen (P2H) process is not considered, and traditional EL and MR are employed for P2G and LTCTM scheme.
Scenario 4: Seasonal hydrogen energy utilization is considered in the LTCTM scheme, but the objective function does not involve carbon trading costs.
Scenario 5: A traditional fixed carbon trading model is employed.
Scenario 6: Both seasonal hydrogen energy utilization and the LTCTM scheme are employed, which is the proposed scheduling plan.

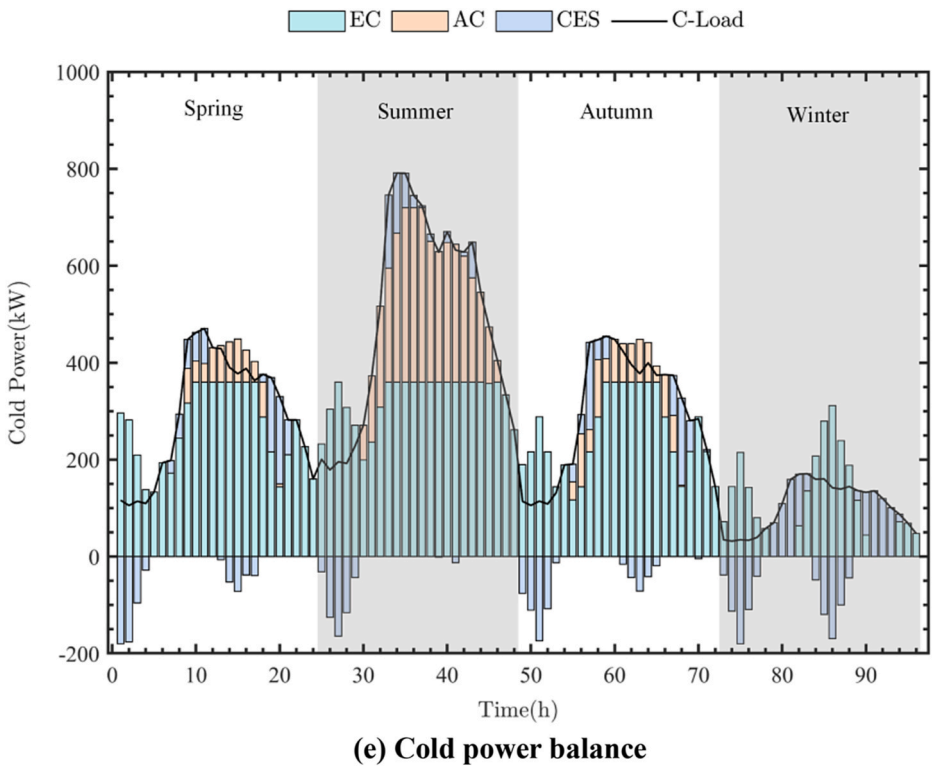

(e) Cold power balance

Fig. 6. (*continued*).

The scenarios for demonstrating the day-ahead scheduling are given in Table 1.

4.2.1. Economic analysis of different cases

To better evaluate the cross-seasonal scheduling characteristics of the system, the scheduling results were calculated based on the average cost of typical daily scheduling over a year in different scenarios. The economic cost of system scheduling for each scenario is shown in Table 2. Scenario 1, due to its complete disregard for refined hydrogen energy utilization, struggles to achieve supply and demand balance, resulting in a significant loss of wind, solar, and load. In Scenario 2, only short-term hydrogen storage was adopted to meet system demand, leading to reduced flexibility in schedule and increased dependence on external energy purchases. Purchase and maintenance costs increase by 4% and 0.7%, respectively, compared to Scenario 6. This indicates that long-term hydrogen storage can enhance economic efficiency. Scenario 3, like Scenario 1, lacks FC compensation for thermal energy supply, leading to significant thermal load shedding. In Scenario 4 where the economic aspect was prioritized, low-cost natural gas was purchased more, leading to a substantial increase in carbon emissions (i.e., 14.3% more than in Scenario 6). Scenarios 5 and 6 yield the closest scheduling results, but the traditional fixed carbon price trading of Scenario 5 is less responsive to carbon emission adjustments, leading to higher carbon emissions and trading costs. The scheduling method that takes into account seasonal hydrogen energy utilization and LTCTM enhances the adjustability and flexibility of the HIES. It effectively promotes interactive regulation between various energy conversion devices and multiple energy sources. Therefore, Scenario 6 has the best overall cost-effectiveness, with total costs reduced by 2.6% and 1% compared to Scenarios 2 and 5, respectively.

To further illustrate the impact of seasonal hydrogen utilization on the scheduling optimization of IES, the operation of the system with varying proportions of seasonal hydrogen storage capacity is optimized. The results respectively display the total cost, purchase cost, and wind and solar power curtailment of the IES with 0%, 33%, 66%, and 100% capacity of seasonal hydrogen storage, as shown in Fig. 5. It is evident that as the increase of seasonal hydrogen utilization, the system's total cost, purchase cost, and wind and solar power loss all decrease. This indicates that seasonal hydrogen utilization can enhance the utilization of renewable energy sources in IES, reduce the amount of energy purchased from the grid, and thereby lower operational costs. However, there is also a clear marginal effect associated with seasonal hydrogen storage. As capacity increases, the cost reduction and wind and solar power absorption gradually diminish. Therefore, it is crucial to equip the IES with a reasonable capacity of seasonal hydrogen storage to maintain a balance between cost reduction and efficiency enhancement.

4.2.2. Results of day-ahead scheduling optimization

Fig. 6(a) to Fig. 6(e) display the optimization results of various forms of energy for the HIES scheduling plan across four typical seasonal days. The balance of electric power shows that during periods of low electricity prices (1:00–5:00 and 22:00–24:00) and insufficient renewable energy supply, the system purchases large amounts of electricity to meet load demands. During midday, when supply from PV and WT is ample, HIES purchases less energy from the external. GT and FC compensate the electrical network as per the actual scheduling situation. The hydrogen balance illustrates that EL increases its operation power during times of surplus electricity or renewable energy generation, converting excess electrical energy into hydrogen for use within other energy flow systems. The system's natural gas purchases are influenced by peak and off-peak gas prices but remain high due to the significant demand from GB and GT. MR and FC increase output power when hydrogen supply is abundant, meeting hydrogen load demands and providing energy in other forms. To maintain thermal balance, GT and GB are mainly used for thermal energy demand, with the remainder supplied by FC. For cold load supply in the HIES, EC is more economical, supplemented by AC. The five types of energy storage exhibit similar patterns in the optimization results: Discharging during energy shortages and charging during surpluses, demonstrating their role in peak shaving and enhancing system economic stability.

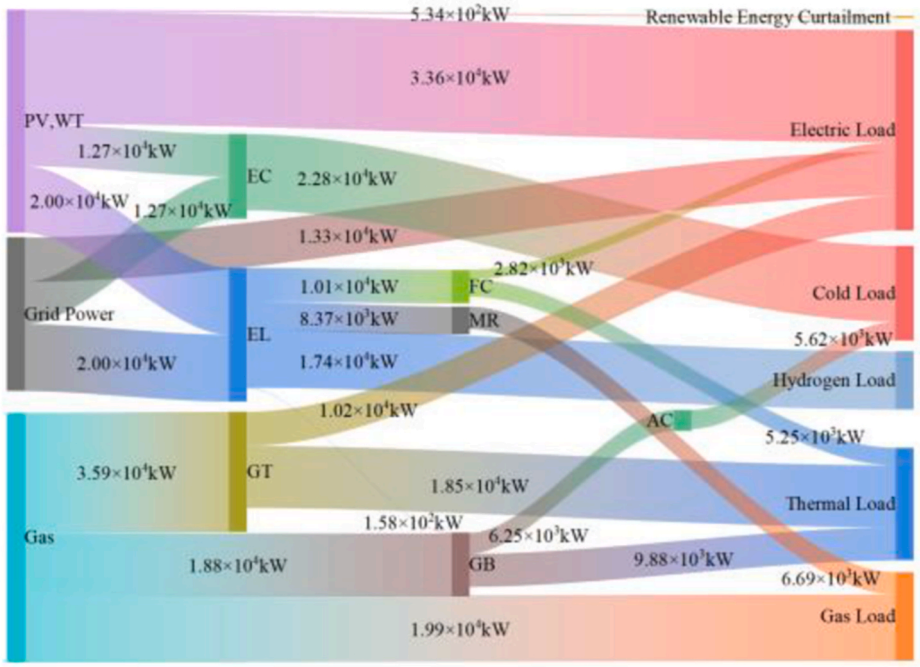

(a) HIES

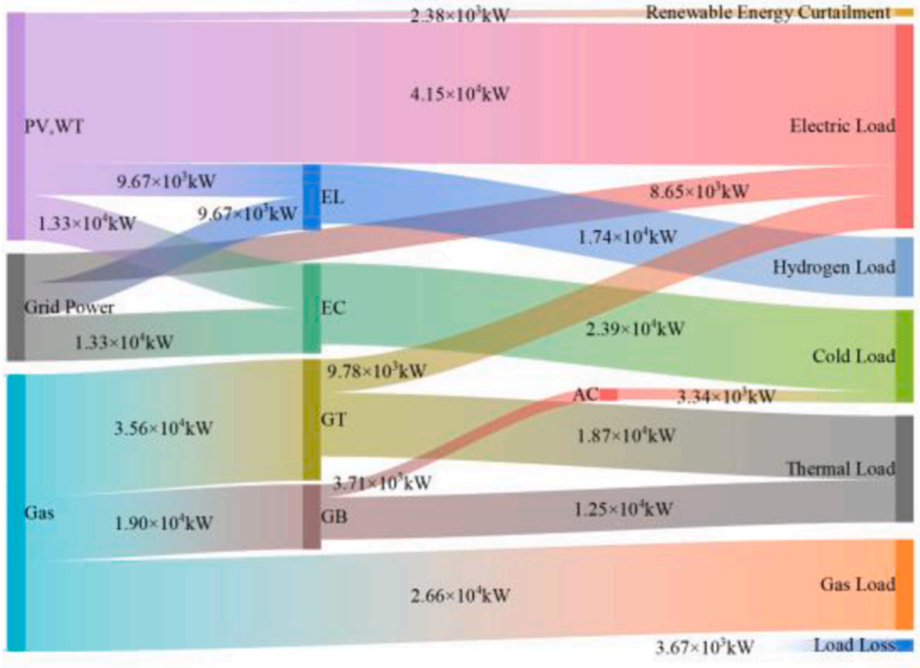

(b) IES without hydrogen network

Fig. 7. Energy flow diagram of the system.

The scheduling results also highlight the HIES's seasonal advantages, especially in thermal and cold energy forms. In typical summer days, the system increases MR and AC output, utilizing hydrogen energy for cooling, thus enhancing the system's cooling capacity. Conversely, on typical winter days, the system adapts accordingly – EC output decreases, and excess electricity is diverted to hydrogen production for FC, which in turn increases thermal output, enhancing the system's thermal supply capacity.

From the analysis, multi-energy flow HIES scheduling on large temporal and spatial scales is the result of multiple device coordination. On the one hand, influenced by renewable energy supply fluctuations and energy prices, the system can arrange scheduling plans rationally by

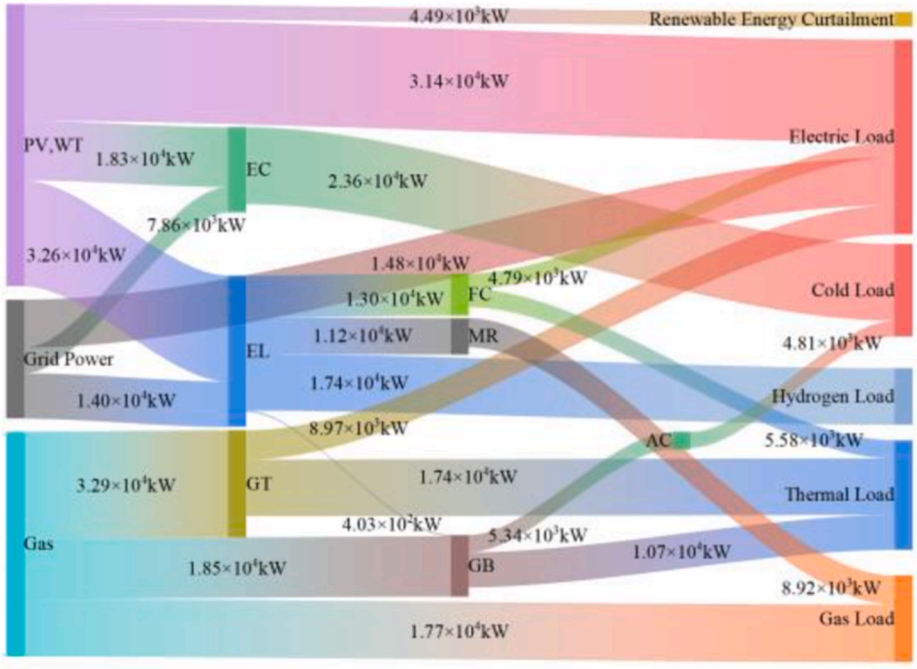

(a) HIES

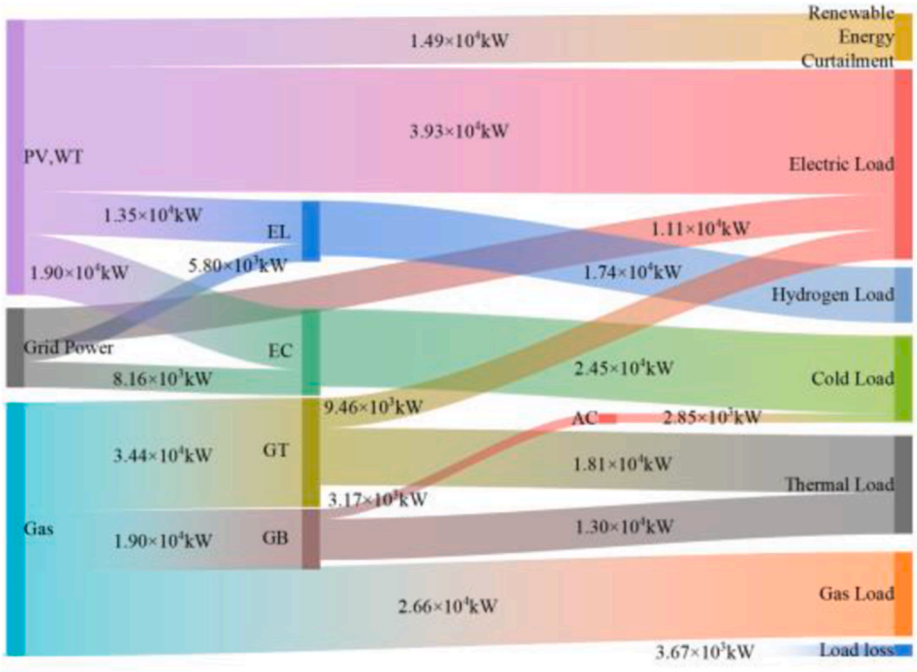

(b) IES without hydrogen network

Fig. 8. Energy flow diagram of the system after increasing wind and solar power generation.

leveraging coordination among energy input, production, conversion, storage, and consumption. Therefore, it promotes efficient renewable energy consumption and the internal energy supply-demand balance of HIES, leading to increased system economic efficiency. On the other hand, considering seasonal hydrogen energy utilization provides an additional method for energy supply-demand balance, improving the system's adaptability and resilience to seasonal and large-scale load changes.

4.2.3. Influences of high penetration level of wind and solar

Fig. 7 illustrates the overall energy flow of the HIES on a typical day, compared to the IES without hydrogen utilization. The most direct and effective means of meeting electric and gas load demands is to purchase electricity from renewable generation and gas from natural gas pipelines. In the HIES, the penetration level of supply from these sources reached 58.8% for electricity and 74.8% for gas, with the remainder being flexibly supplemented by other equipment. This is because direct supply avoids the energy conversion losses associated with intermediate

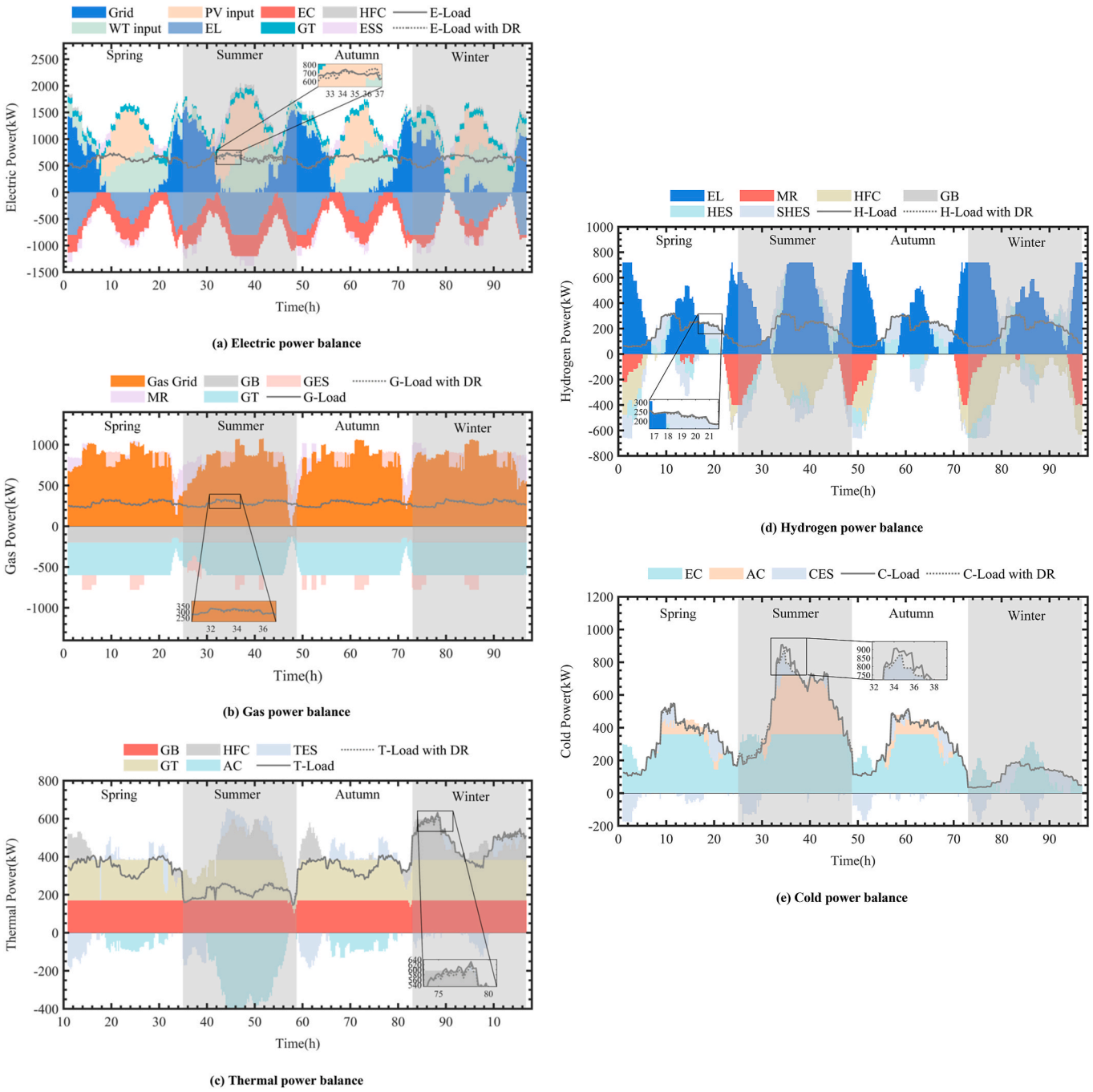

Fig. 9. Energy supply and demand scheduling results of HIES in the intraday stage.

equipment, thus enhancing system efficiency and economy. The supply of heat and cold primarily considers GT, GB, and EC, with their supply penetration level reaching 84.4% and 80.2%, respectively. The EL is the core of the hydrogen network in HIES, and the hydrogen produces not only the needs to meet the system's hydrogen load demand but also ensures sufficient supply for other equipment. The traditional network experienced a load reduction of 3.67×10^3 kW and a renewable energy curtailment of 2.38×10^3 kW, whereas the proposed HIES completely met the system load demand with ignorable curtailment. Compared to an IES without a hydrogen network, the incorporation of the hydrogen chain in HIES is beneficial for overall energy flow, significantly enhancing the capability to adopt more renewable energy.

To further demonstrate the scheduling optimization and high penetration level of wind and solar energy in the HIES, the total input of wind and solar energy was increased by 30%, and the same method was applied to reschedule both systems. The results, as shown in Fig. 8, indicate that with increased renewable energy supply, the overall purchase of energy was reduced in both systems. However, the IES without a hydrogen network still exhibited load shedding. It failed to balance the demand and supply, and the total renewable energy had to be curtailed again by 12,520 kW. Although the HIES also experienced a slight increase in renewable energy curtailment, compared to the IES, its renewable energy penetration level was increased by 12%, and it managed to avoid load shedding, ensuring a balance between supply and demand on both sides of the source and load. Furthermore, with the presence of the hydrogen network, the EL, FC, and MR adaptively increased their power outputs. The overall energy utilization efficiency is increased and the system operational costs are reduced, thus

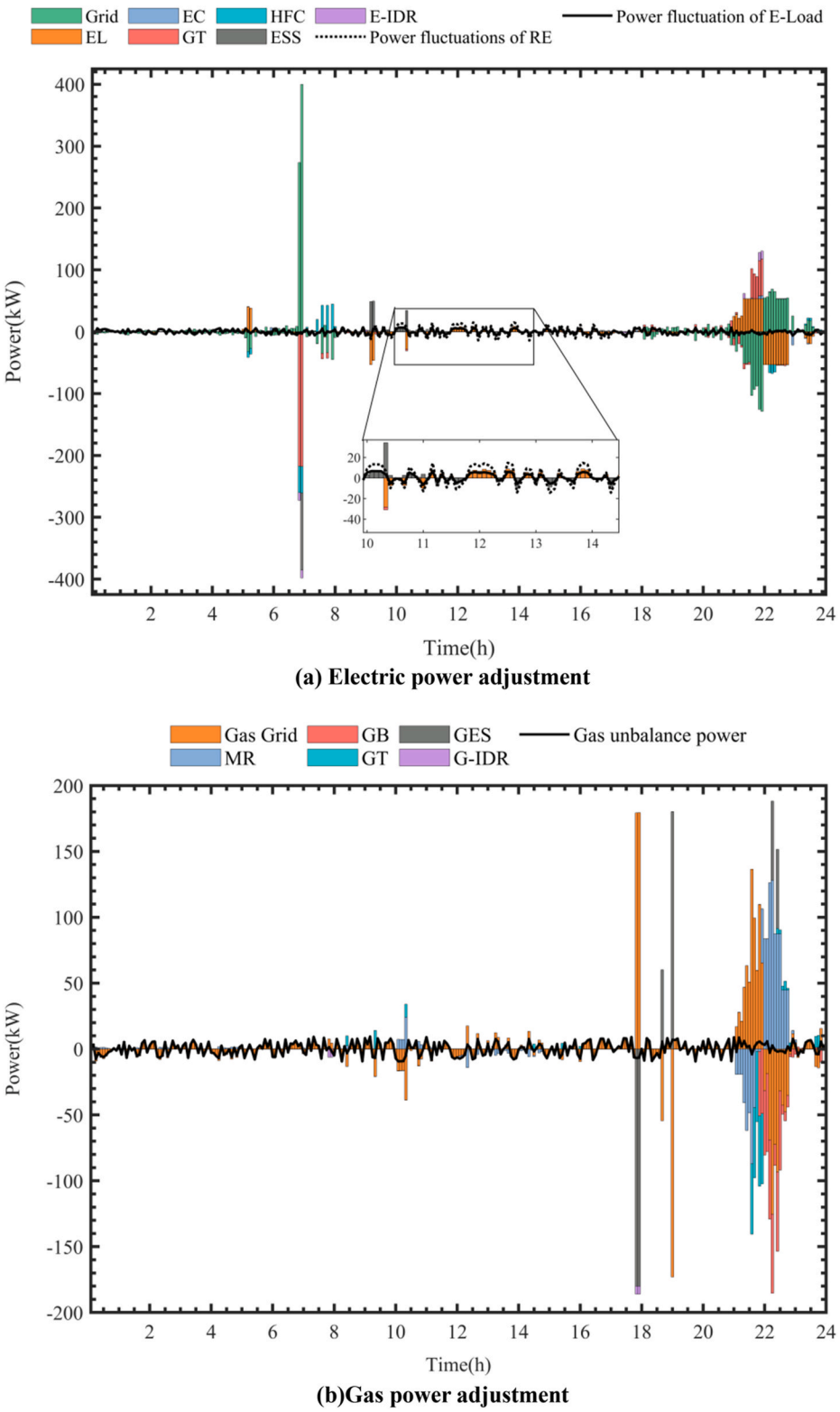

Fig. 10. Power imbalance adjustment for real-time scheduling optimization.

demonstrating the capability to consume a significant level of renewable energy.

4.3. Intraday rolling scheduling analysis

Intraday rolling scheduling refines the day-ahead scheduling results by shortening the time scale and adjusting the output power of various devices. It also considers ADR and IDR, using intraday rolling optimization to further optimize the scheduling results. The energy supply and demand scheduling results for the intraday rolling stage are presented in Fig. 9.

The HIES attempts to find a balance of multiple energy forms at the

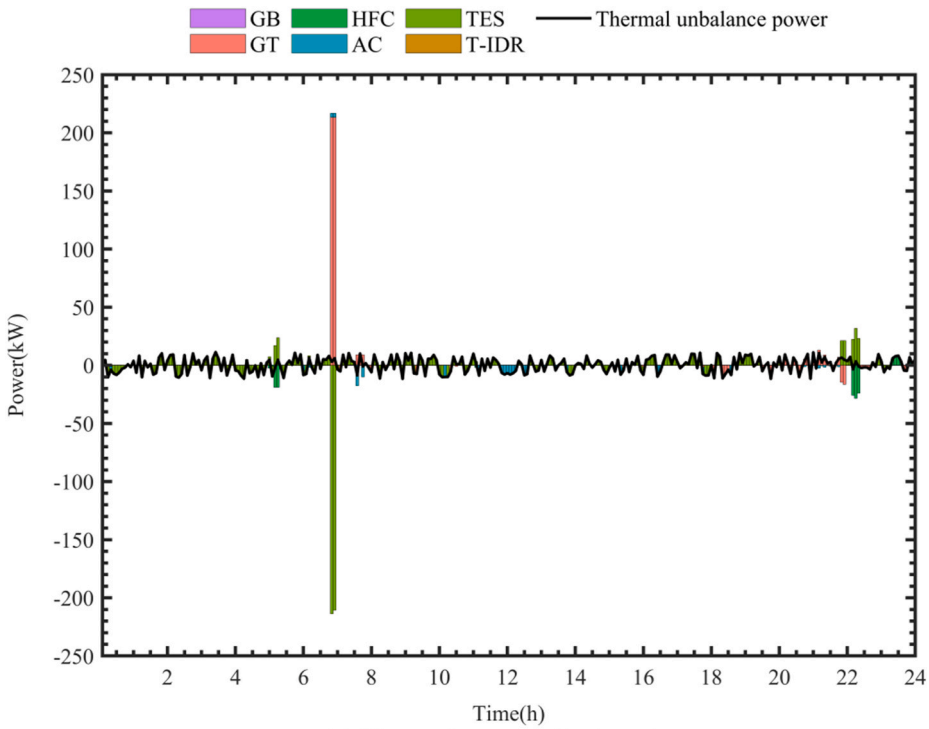

(c) Thermal power adjustment

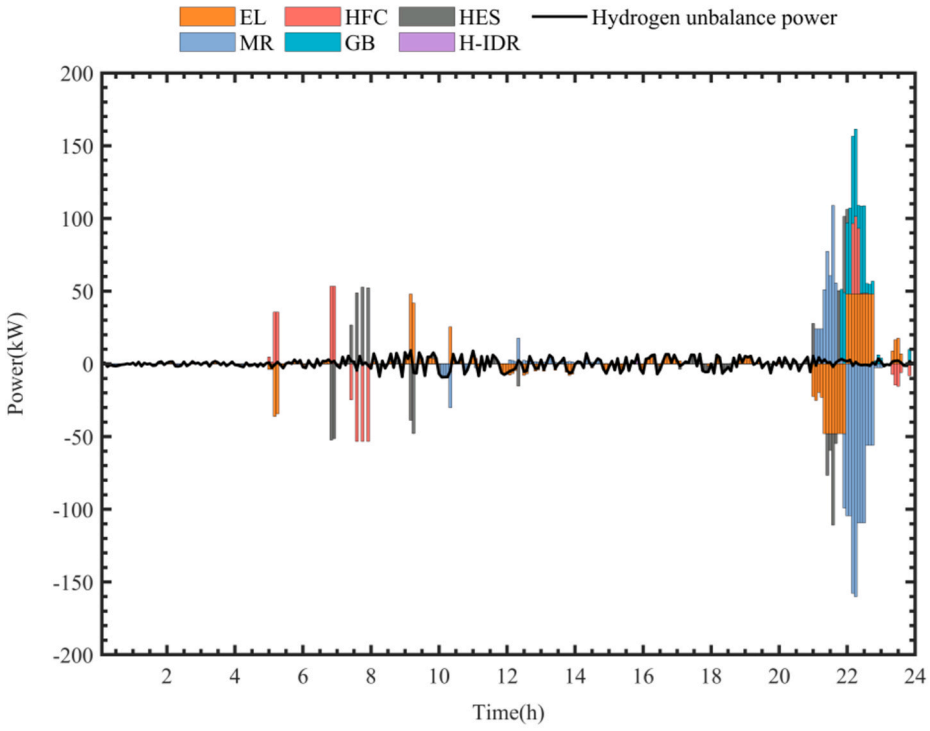

(d) Hydrogen power adjustment

Fig. 10. (*continued*).

intraday stage. However, there are noticeable differences between intraday rolling and day-ahead scheduling plans, especially in minor energy forms, i.e., heat, hydrogen, and cold energy. This is because the prediction accuracy at the intraday stage is higher than in the day-ahead stage, and scheduling changes have a more significant impact on the energy forms of insignificant amounts. Likewise, the power scheduling of various types of energy storage also shows significant changes due to the reduction in time scale. The flexibility of energy storage devices in charging and discharging makes them more sensitive to short-term supply and demand fluctuations. The solid and dashed lines in the intraday scheduling results represent the load changes before and after the inclusion of DR into the model. All types of loads have been reduced during peak energy usage periods through IL, and electricity loads have also been shifted from peak periods to off-peak periods through CL. This

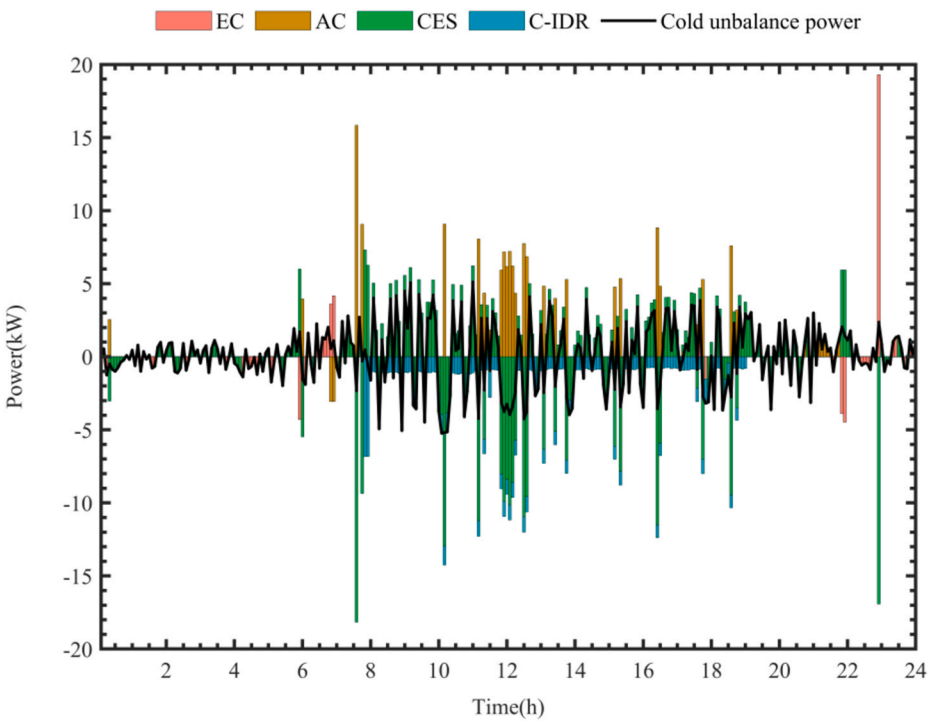

(e) Cold power adjustment

Fig. 10. (*continued*).

Table 3
Scheduling results at different time scales.

Time scale	Purchase cost (¥)	Maintenance cost (¥)	Carbon emissions (¥)	Remaining costs (¥)	Total cost (¥)
Day-ahead schedule	14,679	1416	3454	27	19,576
Intraday schedule	14,662	1423	3663	571	20,318
Real-time schedule	14,674	1424	3655	440	20,193

demonstrates that the implementation of IDR reduces the energy supply burden on the system and enhances the economic efficiency of HIES.

4.4. Real-time scheduling analysis

4.4.1. Analysis of system imbalance for real-time scheduling

The results of power fluctuation adjustments during the real-time stage are illustrated using a typical summer day, as shown in Fig. 10. The power imbalance in the real-time stage primarily results from fluctuations in WT, PV, and five types of loads. Due to the short time intervals in real-time scheduling, the system's DR only considers IDR adjustments. The HIES addresses energy supply and demand balance by prioritizing energy storage adjustments and flexible energy conversion equipment. On the demand side, it is necessary to consider the amount of scheduling and costs to adaptively adjust the size of the IDR. Table 3 presents the cost of HIES-optimized scheduling across different time scales. Compared to the day-ahead schedule, real-time scheduling is more refined, resulting in less external energy purchasing. Although the total cost is relatively higher, it includes adjustment costs and IDR, which are not present in the day-ahead phase. Compared to the intraday stage, WT, PV, and load deviations are lower in real-time scheduling. The adjustments in HIES's output plan aim to achieve power balance during the real-time stage, reducing the remaining costs by 30%, with purchase costs, maintenance costs, and carbon trading costs remaining essentially unchanged.

4.4.2. Analysis of multiple demand responses

It is important to note that as the demand side plays an increasingly significant role in the optimized operation and energy allocation of HIES, the time characteristics of DR also deserve considerable attention. For instance, the effects of multiple demand responses in different energy forms and scales were investigated on a typical summer day, and the results are depicted in the waterfall comparison charts in Fig. 11. Each chart displays the comparative results of all forms of DR for that particular energy type, reflecting the impact of DR on scheduling at different time scales.

As commodity energy, both electricity and gas are suitable for PDR. PDR adjusts according to energy prices, reducing loads when prices are high and increasing loads when prices are low, thereby reducing system costs and improving economic efficiency. Electric and cold loads use ADR, characterized by a reduction in electric and cold loads during peak periods, while gas and heat loads experience a corresponding increase, effectively substituting a portion of electric and cold loads with gas and heat loads. IDR, with the highest operability among all DR types, is involved in the adjustment of all five types of loads. In terms of time scale, PDR has the longest adjustment scale, covering the entire period of high and low energy purchase prices. ADR adjusts at the day-ahead and intraday time scales, covering a smaller range than PDR. IDR has the smallest time scale for adjustment, meeting the demand response needs of intraday and real-time stages with sensitive and high-frequency curve changes.

In summary, multiple demand responses are involved in HIES scheduling optimization through energy prices and incentive signals,

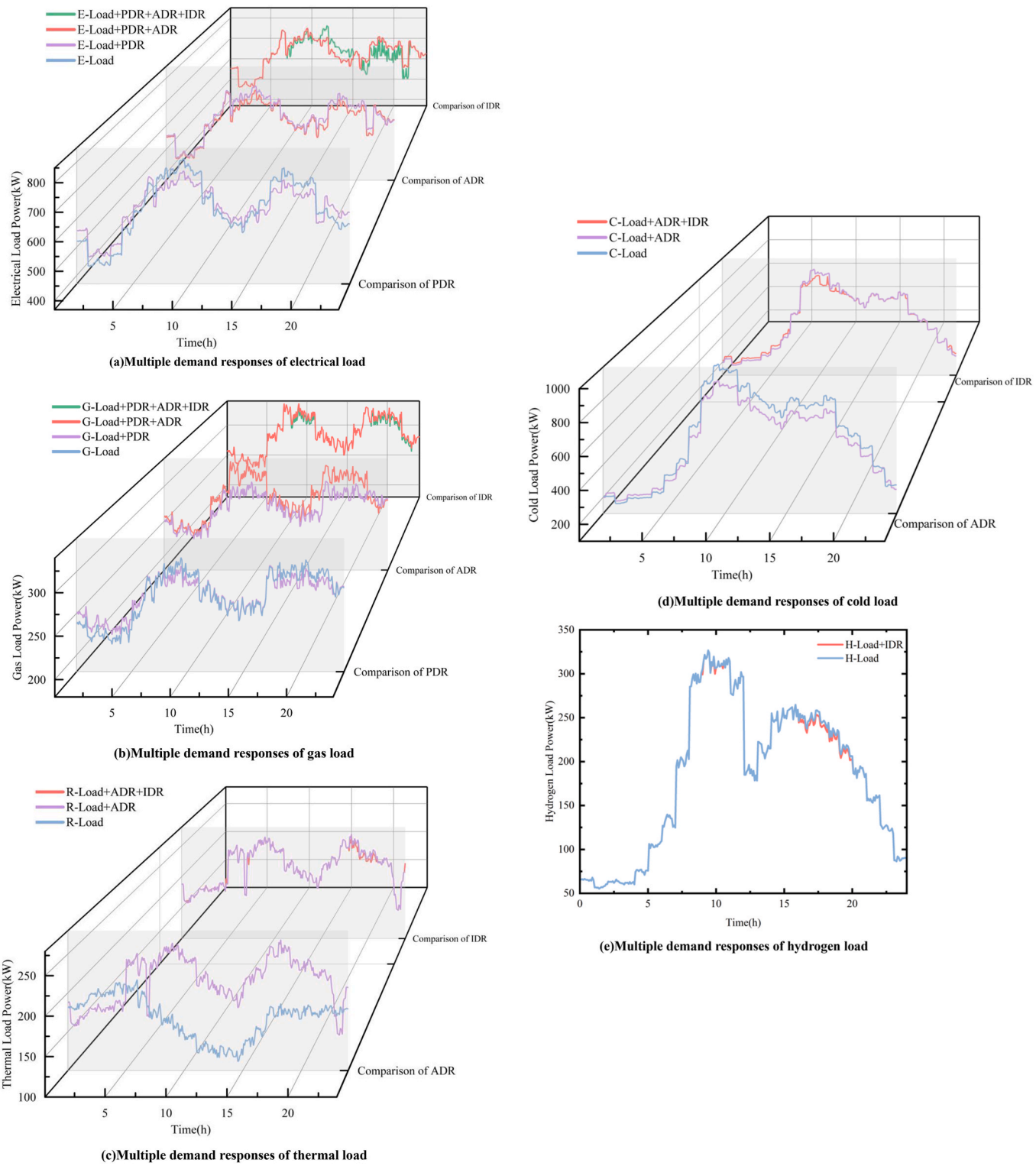

Fig. 11. Comparison of multiple demand responses.

optimize load curve distribution, reduce system costs, and improve system energy efficiency. Furthermore, different types of demand responses exhibit distinct time distribution characteristics. Selecting appropriate DR types based on the adjustment time scale in practical engineering applications helps to improve the supply-demand balance and enhance the system's economic performance.

5. Conclusion

This paper proposes an operational strategy based on multi-time scale scheduling optimization for HIES. Seasonal hydrogen energy utilization and multiple demand responses are considered in a three-stage optimization process. The strategy is validated using historical weather and operational data from South China with a monsoon climate. In the day-ahead scheduling stage, the data are used to cluster and analyze the

typical daily input power of the HIES across all seasons, taking into account the LTCTM. A mixed-integer nonlinear model is established for HIES based on the utilization of seasonal hydrogen energy. In the intraday phase, the scheduling plan of the day-ahead phase is used as a reference, considering 15-min level forecast values and a rolling optimization model incorporating ADR and IDR is established. In the real-time phase, the scheduling plan from the intraday stage is adopted, and a chance-constrained method is designed for refined scheduling solutions, taking into account changes in the 5-min level time scale and IDR mechanisms. The results show that the comprehensive utilization of seasonal hydrogen energy and the LTCTM are more efficient and stable in meeting system operation and supply-demand balance, and the total operational costs can be reduced by 2.6% and 1%, respectively.

Furthermore, renewable energy generation and load changes have significant seasonal characteristics. Considering seasonal energy storage and hydrogen utilization enhances self-regulation capability in response to load variations. In addition, refined hydrogen energy utilization improves the overall energy flow in the HIES. The ability to consume renewable energy generation is increased by 12% compared to traditional systems, significantly enhancing the system's energy utilization efficiency.

The successful implementation of DR requires guidance from government policies, effective operation by power system operators, and active participation from users. Various types of DR strategies exhibit significant differences in their suitability concerning time scales and load types. In practical systems, the implementation of different types of DR can be adjusted to balance between system economy and reliability.

It is important to point out that the proposed method of model reformulation and solution through piecewise linearization is only validated for linearized models and low-degree polynomial models. However, the output characteristics of system equipment in practical applications may exhibit strong nonlinearity and are closely related to time-varying dynamic characteristics. Therefore, more detailed models and more sophisticated solution methods, possibly combined with intelligent algorithms, need to be further developed, which can be the direction for future research in this area.

Declaration of competing interest

The authors declare that they have no known competing financial interests or personal relationships that could have appeared to influence the work reported in this paper.

CRediT authorship contribution statement

Zhewei Wang: Writing – original draft, Investigation, Data curation. **Banghua Du:** Software, Methodology, Data curation. **Yang Li:** Writing – review & editing, Supervision. **Changjun Xie:** Writing – review & editing, Supervision, Funding acquisition, Conceptualization. **Han Wang:** Validation, Formal analysis. **Yunhui Huang:** Visualization, Software. **Peipei Meng:** Resources, Project administration.

Acknowledgement

This work was supported by the National Key Research and Development Program of China (2020YFB1506802).

Appendix A. Supplementary data

Supplementary data to this article can be found online at https://doi.org/10.1016/j.ijhydene.2024.04.125.

References

[1] Zhang C, Xu Y, Dong ZY. Robustly coordinated operation of a multi-energy microgrid in grid-connected and islanded modes under uncertainties. IEEE Trans Sustain Energy 2020;11(2):640–51. https://doi.org/10.1109/TSTE.2019.2900082.
[2] Wan W, Yang Y, Li Y, Xie C, Song J, Deng Z, Zhang R. Operating conditions combination analysis method of optimal water management state for PEM fuel cell. Green Energy and Intelligent Transportation 2023;2(4). https://doi.org/10.1016/j.geits.2023.100105.
[3] Hong B, Chen J, Zhang W, Shi Z, Li J, Miao W. Integrated energy system planning at modular regional-user level based on a two-layer bus structure. CSEE Journal of Power and Energy Systems 2018;4(2):188–96. https://doi.org/10.17775/cseejpes.2018.00110.
[4] Zhu X, Gui P, Zhang X, Han Z, Li Y. Multi-objective optimization of a hybrid energy system integrated with solar-wind-PEMFC and energy storage. J Energy Storage 2023;72:108562. https://doi.org/10.1016/j.est.2023.108562. Retrieved from, https://www.sciencedirect.com/science/article/pii/S2352152X2301959X.
[5] Cheng S, Wang R, Xu J, Wei Z. Multi-time scale coordinated optimization of an energy hub in the integrated energy system with multi-type energy storage systems. Sustain Energy Technol Assessments 2021;47. https://doi.org/10.1016/j.seta.2021.101327.
[6] Liu S, Yan J, Yan Y, Zhang H, Zhang J, Liu Y, Han S. Joint operation of mobile battery, power system, and transportation system for improving the renewable energy penetration rate. Appl Energy 2024;357:122455. https://doi.org/10.1016/j.apenergy.2023.122455. Retrieved from, https://www.sciencedirect.com/science/article/pii/S0306261923018196.
[7] Yu B, Fang D, Xiao K, Pan Y. Drivers of renewable energy penetration and its role in power sector's deep decarbonization towards carbon peak. Renew Sustain Energy Rev 2023;178:113247. https://doi.org/10.1016/j.rser.2023.113247. Retrieved from, https://www.sciencedirect.com/science/article/pii/S136403212300103X.
[8] Bartolini A, Carducci F, Muñoz CB, Comodi G. Energy storage and multi energy systems in local energy communities with high renewable energy penetration. Renew Energy 2020;159:595–609. https://doi.org/10.1016/j.renene.2020.05.131. Retrieved from, https://www.sciencedirect.com/science/article/pii/S0960148120308351.
[9] Shi M, Wang H, Xie P, Lyu C, Jian L, Jia Y. Distributed energy scheduling for integrated energy system clusters with peer-to-peer energy transaction. IEEE Trans Smart Grid 2023;14(1):142–56. https://doi.org/10.1109/TSG.2022.3197435.
[10] Liu J, Li Y, Ma Y, Qin R, Meng X, Wu J. Two-layer multiple scenario optimization framework for integrated energy system based on optimal energy contribution ratio strategy. Energy 2023;285:128673. https://doi.org/10.1016/j.energy.2023.128673. Retrieved from, https://www.sciencedirect.com/science/article/pii/S0360544223020674.
[11] Yang X, Wang X, Deng Y, Mei L, Deng F, Zhang Z. Integrated energy system scheduling model based on non-complete interval multi-objective fuzzy optimization. Renew Energy 2023;218:119289. https://doi.org/10.1016/j.renene.2023.119289. Retrieved from, https://www.sciencedirect.com/science/article/pii/S0960148123012041.
[12] Geidl M, Koeppel G, Favre-Perrod P, Kloeckl B, Andersson G, Froehlich K. Energy hubs for the future. IEEE Power Energy Mag 2007;5(1):24–30. https://doi.org/10.1109/mpae.2007.264850. Retrieved from <Go to ISI>://WOS:000249965500008.
[13] Wang Y, Zhang N, Kang C, Kirschen DS, Yang J, Xia Q. Standardized matrix modeling of multiple energy systems. IEEE Trans Smart Grid 2019;10(1):257–70. https://doi.org/10.1109/tsg.2017.2737662. Retrieved from <Go to ISI>://WOS:000455180900024.
[14] Cheng S, Wang R, Xu J, Wei Z. Multi-time scale coordinated optimization of an energy hub in the integrated energy system with multi-type energy storage systems. Sustain Energy Technol Assessments 2021;47:101327. https://doi.org/10.1016/j.seta.2021.101327. Retrieved from, https://www.sciencedirect.com/science/article/pii/S2213138821003374.
[15] Wang Y, Hu J, Liu N. Energy management in integrated energy system using energy–carbon integrated pricing method. IEEE Trans Sustain Energy 2023;14(4):1992–2005. https://doi.org/10.1109/TSTE.2023.3295573.
[16] Xu J, Wang J, Chen Y, Xu Z, Lund PD. Thermo-ecological cost optimization of a solar thermal and photovoltaic integrated energy system considering energy level. Sustain Prod Consum 2022;33:298–311. https://doi.org/10.1016/j.spc.2022.07.011. Retrieved from, https://www.sciencedirect.com/science/article/pii/S2352550922001853.
[17] Li P, Wang Z, Yang W, Liu H, Yin Y, Wang J, Guo T. Hierarchically partitioned coordinated operation of distributed integrated energy system based on a master-slave game. Energy 2021;214. https://doi.org/10.1016/j.energy.2020.119006.
[18] Li G, Zhang R, Jiang T, Chen H, Bai L, Li X. Security-constrained bi-level economic dispatch model for integrated natural gas and electricity systems considering wind power and power-to-gas process. Appl Energy 2017;194:696–704. https://doi.org/10.1016/j.apenergy.2016.07.077.
[19] Ma Y, Wang H, Hong F, Yang J, Chen Z, Cui H, Feng J. Modeling and optimization of combined heat and power with power-to-gas and carbon capture system in integrated energy system. Energy 2021;236. https://doi.org/10.1016/j.energy.2021.121392.
[20] Li X, Wang W, Wang H. Hybrid time-scale energy optimal scheduling strategy for integrated energy system with bilateral interaction with supply and demand. Appl Energy 2021;285. https://doi.org/10.1016/j.apenergy.2021.116458.
[21] Deng H, Wang J, Shao Y, Zhou Y, Cao Y, Zhang X, Li W. Optimization of configurations and scheduling of shared hybrid electric-hydrogen energy storages supporting to multi-microgrid system. J Energy Storage 2023;74:109420. https://

doi.org/10.1016/j.est.2023.109420. Retrieved from, https://www.sciencedirect.com/science/article/pii/S2352152X23028189.
[22] Zhang Y, Hua QS, Sun L, Liu Q. Life cycle optimization of renewable energy systems configuration with hybrid battery/hydrogen storage: a comparative study. J Energy Storage 2020;30:101470. https://doi.org/10.1016/j.est.2020.101470. Retrieved from, https://www.sciencedirect.com/science/article/pii/S2352152X20303030.
[23] Shi T, Xu C, Dong W, Zhou H, Bokhari A, Klemeš JJ, Han N. Research on energy management of hydrogen electric coupling system based on deep reinforcement learning. Energy 2023;282:128174. https://doi.org/10.1016/j.energy.2023.128174. Retrieved from, https://www.sciencedirect.com/science/article/pii/S0360544223015682.
[24] Wang S, Wang S, Zhao Q, Dong S, Li H. Optimal dispatch of integrated energy station considering carbon capture and hydrogen demand. Energy 2023;269. https://doi.org/10.1016/j.energy.2023.126981.
[25] Wu Q, Li C. Modeling and operation optimization of hydrogen-based integrated energy system with refined power-to-gas and carbon-capture-storage technologies under carbon trading. Energy 2023;270. https://doi.org/10.1016/j.energy.2023.126832.
[26] He J, Wu Y, Yong X, Tan Q, Liu F. Bi-level optimization of a near-zero-emission integrated energy system considering electricity-hydrogen-gas nexus: a two-stage framework aiming at economic and environmental benefits. Energy Convers Manag 2022;274. https://doi.org/10.1016/j.enconman.2022.116434.
[27] Klyapovskiy S, Zheng Y, You S, Bindner HW. Optimal operation of the hydrogen-based energy management system with P2X demand response and ammonia plant. Appl Energy 2021;304:117559. https://doi.org/10.1016/j.apenergy.2021.117559. Retrieved from, https://www.sciencedirect.com/science/article/pii/S0306261921009375.
[28] Liu Z, Fan G, Meng X, Hu Y, Wu D, Jin G, Li G. Multi-time scale operation optimization for a near-zero energy community energy system combined with electricity-heat-hydrogen storage. Energy 2024;291. https://doi.org/10.1016/j.energy.2024.130397.
[29] Dong H, Fu Y, Jia Q, Zhang T, Meng D. Low carbon optimization of integrated energy microgrid based on life cycle analysis method and multi time scale energy storage. Renew Energy 2023;206:60–71. https://doi.org/10.1016/j.renene.2023.02.034.
[30] Pan C, Fan H, Zhang R, Sun J, Wang Y, Sun Y. An improved multi-timescale coordinated control strategy for an integrated energy system with a hybrid energy storage system. Appl Energy 2023;343. https://doi.org/10.1016/j.apenergy.2023.121137.
[31] Cheng Z, Jia D, Li Z, Xu S, Si J. Multi-time-scale energy management for microgrid using expected-scenario-oriented stochastic optimization. Sustainable Energy, Grids and Networks 2022;30. https://doi.org/10.1016/j.segan.2022.100670.
[32] Wang X, Han L, Wang C, Yu H, Yu X. A time-scale adaptive dispatching strategy considering the matching of time characteristics and dispatching periods of the integrated energy system. Energy 2023;267. https://doi.org/10.1016/j.energy.2022.126584.
[33] Wang Z, Tao H, Cai W, Duan Y, Wu D, Zhang L. Study on the multitime scale rolling optimization operation of a near-zero energy building energy supply system. Energy Convers Manag 2022;270. https://doi.org/10.1016/j.enconman.2022.116255.
[34] Wang L, Lin J, Dong H, Wang Y, Zeng M. Demand response comprehensive incentive mechanism-based multi-time scale optimization scheduling for park integrated energy system. Energy 2023;270. https://doi.org/10.1016/j.energy.2023.126893.
[35] Li P, Wang Z, Wang J, Guo T, Yin Y. A multi-time-space scale optimal operation strategy for a distributed integrated energy system. Appl Energy 2021;289. https://doi.org/10.1016/j.apenergy.2021.116698.
[36] Ma K, Zhang R, Yang J, Song D. Collaborative optimization scheduling of integrated energy system considering user dissatisfaction. Energy 2023;274. https://doi.org/10.1016/j.energy.2023.127311.
[37] Tan C, Geng S, Zhao Z, Tan Z. Multi time scale operation optimization of EHHGS considering equipment uncertainty and response characteristics. J Clean Prod 2023;382. https://doi.org/10.1016/j.jclepro.2022.135106.
[38] Xiang Y, Cai H, Gu C, Shen X. Cost-benefit analysis of integrated energy system planning considering demand response. Energy 2020;192:116632. https://doi.org/10.1016/j.energy.2019.116632. Retrieved from, https://www.sciencedirect.com/science/article/pii/S0360544219323278.
[39] Wang X, Bie Z, Liu F, Kou Y, Jiang L. Bi-level planning for integrated electricity and natural gas systems with wind power and natural gas storage. Int J Electr Power Energy Syst 2020;118:105738. https://doi.org/10.1016/j.ijepes.2019.105738. Retrieved from, https://www.sciencedirect.com/science/article/pii/S0142061519326444.
[40] Lei D, Zhang Z, Wang Z, Zhang L, Liao W. Long-term, multi-stage low-carbon planning model of electricity-gas-heat integrated energy system considering ladder-type carbon trading mechanism and CCS. Energy 2023;280. https://doi.org/10.1016/j.energy.2023.128113.
[41] Li Y, Bu F, Gao J, Li G. Optimal dispatch of low-carbon integrated energy system considering nuclear heating and carbon trading. J Clean Prod 2022;378. https://doi.org/10.1016/j.jclepro.2022.134540.
[42] Kirschen DS, Strbac G, Cumperayot P, Mendes DdP. Factoring the elasticity of demand in electricity prices. IEEE Trans Power Syst 2000;15(2):612–7. https://doi.org/10.1109/59.867149.
[43] Li P, Wang Z, Wang J, Yang W, Guo T, Yin Y. Two-stage optimal operation of integrated energy system considering multiple uncertainties and integrated demand response. Energy 2021;225. https://doi.org/10.1016/j.energy.2021.120256.
[44] Li R, Smith N, Li F. Multi-resolution load profile clustering for smart metering data. In: Paper presented at the 2017 IEEE power & energy society general meeting; 2017. 16-20 July 2017.